MISCELLANEOUS PAPER S-70-3

SEEPAGE IN MISSISSIPPI RIVER BANKS

Report 1

ANALYSIS OF TRANSIENT SEEPAGE USING VISCOUS FLOW MODEL AND NUMERICAL METHODS

by

C. S. Desai

February 1970

Sponsored by U. S. Army Engineer Division, Lower Mississippi Valley

Conducted by U. S. Army Engineer Waterways Experiment Station, Vicksburg, Mississippi

MISCELLANEOUS PAPER S-70-3

SEEPAGE IN MISSISSIPPI RIVER BANKS

Report 1

ANALYSIS OF TRANSIENT SEEPAGE USING VISCOUS FLOW MODEL AND NUMERICAL METHODS

by

C. S. Desai

February 1970

Sponsored by U. S. Army Engineer Division, Lower Mississippi Valley

Conducted by U. S. Army Engineer Waterways Experiment Station, Vicksburg, Mississippi

ARMY-MRC VICKSBURG, MISS.

THE CONTENTS OF THIS REPORT ARE NOT TO BE USED FOR ADVERTISING, PUBLICATION, OR PROMOTIONAL PURPOSES. CITATION OF TRADE NAMES DOES NOT CONSTITUTE AN OFFICIAL ENDORSEMENT OR APPROVAL OF THE USE OF SUCH COMMERCIAL PRODUCTS.

FOREWORD

The study of transient seepage in Mississippi River banks was initiated by the U. S. Army Engineer Waterways Experiment Station (WES), Vicksburg, Miss., at the request of the U. S. Army Engineer Division, Lower Mississippi Valley (LMVD).

A viscous flow model was designed and constructed by WES. This report contains experimental results obtained from the model and comparisons of these results with analytical results obtained by employing numerical techniques.

The tests described in this report were conducted by Dr. C. S. Desai and Mr. A. L. Sullivan. Analytical studies were made by Dr. Desai. Some initial study, including development of closed form solutions and preliminary tests, was done by Dr. V. Lakshminarayana. The work was accomplished under the direction of Messrs. W. J. Turnbull, A. A. Maxwell, and W. C. Sherman, Soils Division, WES. This report was prepared by Dr. Desai and was reviewed and approved by the LMVD prior to its publication. Useful comments and suggestions by Messrs. R. I. Kaufman and F. J. Weaver of the LMVD are greatly appreciated.

Directors of the WES during the design and construction of the model, performance of the tests reported herein, and preparation and publication of this report were COL John R. Oswalt, Jr., CE, and COL Levi A. Brown, CE. Technical Directors were Messrs. J. B. Tiffany and F. R. Brown.

CONTENTS

NOTATION

A	Matrix
A_x, A_y	Constants
b	Half width of gap
B	Boundary, matrix
c	Constant, rate of rise of flood
C_x	Constant
D	Matrix, operator, constant
erfc	Error function
exp	Exponential
f	Function
g	Gravitational constant
h	Head, vector, potential
h_o	Maximum upstream head
h_1, h_2	Upstream and downstream heads
$\bar{h}$	Mean head
H	Head, total head
i	Index
I	Modified Bessel function
j	Index
J_s	Bessel function
k	Index, coefficient of permeability (L/T)
k_o	Permeability (L^2)
L	Length of model
L_r	Length scale ratio
m	Coefficient of permeability of gap, index
n	Porosity

p	Pressure, exponent
P	Matrix
q	Rate of flow
Q	Matrix
r	Coordinate
R, RR	Matrix
s	Coordinate, factor
t	Time
T	Period
T_r	Time scale ratio
u	Head, velocity component, function
$\bar{u}$	Mean velocity component
U	Parameter
v	Velocity component
$\bar{v}$	Mean velocity component
V	Volume
V_r	Velocity ratio
w	Velocity component
x	Coordinate
X	Body force component, vector
y	Coordinate
Y	Body force component
z	Coordinate
Z	Body force component
α	Constant, angle
α_1	Constant
β_x, β_y	Factors
γ	Density
Δt	Time interval
Δx	Interval in x direction
Δy	Interval in y direction
θ	Angular coordinate
λ	Constant
μ	Viscosity

ν	Kinematic viscosity
ρ	Mass density
τ	Factor
ψ	Function
ω	Frequency
Ω	Potential function
∇	Operator
∂	Partial differential operator

CONVERSION FACTORS, BRITISH TO METRIC UNITS OF MEASUREMENT

British units of measurement used in this report can be converted to metric units as follows:

Multiply	By	To Obtain
inches	2.54	centimeters
feet	0.3048	meters
square inches	6.4516	square centimeters
pounds per square inch	0.070307	kilograms per square centimeter
Fahrenheit degrees	5/9	Celsius or Kelvin degrees*

* To obtain Celsius (C) temperature readings from Fahrenheit (F) readings, use the following formula: $C = (5/9)(F - 32)$. To obtain Kelvin (K) readings, use: $K = (5/9)(F - 32) + 273.15$.

SUMMARY

The design of stable riverbank slopes along the Mississippi River is dependent upon the seepage conditions within the banks generated by varying river level, including sudden drawdown. Available seepage analyses are not adequate for the determination of the continuously changing free-water surface under time-dependent variations in river levels. A parallel plate viscous flow model was constructed and tested and was found to constitute a reliable means of obtaining the transient free surface within a sloping bank.

Two series of model tests were performed using a vertical upstream face and an upstream slope of 45 deg. The head at the upstream face of the model was allowed to rise at a constant rate.

The experimental results are suitable only for simple boundary conditions and for homogeneous banks. It was, therefore, intended to develop some analytical techniques which can account for complex boundary conditions and nonhomogeneous material properties usually encountered in riverbanks. The finite difference and the finite element methods provide efficient numerical techniques for obtaining numerical solutions. The finite difference method was employed to obtain solutions for one- and two-dimensional flow conditions for a vertical riverbank and a sloping riverbank, respectively. To assess the applicability of the method for complex conditions, the numerical results were compared with those obtained from the experiments with the model for simple conditions. Good agreement was obtained between the two results. The basic formulation of the finite element method was developed and is included in this report.

It is planned to develop some mechanical device to reproduce in the model various conditions of rise and fall of the river. It is recommended that programs for the finite difference and the finite element methods be further developed with an aim toward (a) providing complete solutions for complex boundary conditions and arbitrary variation of material properties encountered in riverbanks, and (b) simulating various types of river stage variations.

SEEPAGE IN MISSISSIPPI RIVER BANKS

ANALYSIS OF TRANSIENT SEEPAGE USING VISCOUS FLOW MODEL AND NUMERICAL METHODS

PART I: INTRODUCTION

1. Prior to revetment construction along the Mississippi River, the riverbank slopes usually must be graded to help ensure their stability under various conditions, including sudden drawdown. Required slopes are computed on the basis of stability analyses. For a sudden fall in the river level, the free-water surface in the earth bank lags behind the falling level of water in the river, and it is generally difficult to compute such a free-water surface in the bank. Conventionally, the free-water surface in the bank is computed on the basis of full drawdown. This procedure, however, is conservative for many cases and requires flatter slopes than necessary.[1]

The Problem

2. The stability of an earth slope subjected to the effects of changing river stages is dependent on, among other factors, the pore pressures induced within the earth mass due to seepage. The pore pressures are generally estimated from flow net analysis obtained under steady state conditions. However, a more precise determination of pore pressures is needed for the case of a continuously moving free surface. In recent years, extensive piezometer installations at selected locations along the banks of the Mississippi River have provided considerable valuable data on the development of free surface and pore pressures as a function of changing river levels.

3. The purpose of this study is to investigate the transient development of pore pressures in an earth bank under conditions of variable rates of rise or fall in river level and to evolve a more rational method for predicting location of free surface and distribution of pore pressures for use in design and stability analysis.

Approach

4. Various methods are available for analyzing the transient seepage phenomenon. The conventional methods are found deficient, since they are based on many simplified assumptions concerning the material behavior, material composition, etc. Closed form analytical solutions can be obtained when the boundary conditions are simple and the earth comprising the bank is homogeneous. For complex boundary conditions and nonhomogeneous materials, closed form solutions become cumbersome and unwieldy to obtain. To account for such conditions, recourse is made to numerical techniques and laboratory model studies.

5. The general differential equation governing the flow of a fluid through porous media is employed to represent, as a special case, the flow of water through a pervious soil comprising a riverbank with different sloping entrance faces. The flow is assumed to be two-dimensional for a riverbank of infinite landward extent. For a bank with a vertical entrance face, the flow condition is further simplified by assuming the flow to be one-dimensional. The finite difference and the finite element techniques are utilized to obtain numerical solutions to the governing differential equations. Both methods can account for nonhomogeneous materials and complex boundary conditions.

6. A Hele-Shaw parallel plate viscous flow model was constructed to allow comparisons between the analytical and observed results. This report contains a description of the model and presents comparisons of results from the finite difference technique for one-dimensional flow conditions and from the viscous flow model with vertical upstream face. Experiments with the model are in progress for various entrance slopes. A brief description of comparisons between the results from two-dimensional finite difference analysis and experiments with an entrance slope of 45 deg is included. Basic formulation for the finite element method for two-dimensional flow conditions is also included.

7. The investigations are in progress, and the future work will involve completion of computer programs for the finite difference and finite element methods. Finally, the observed results will be compared with the

analytical results so as to assess the applicability of analytical results to field problems.

PART II: THEORY AND DESCRIPTION OF MODEL

Theory

Governing equations of flow in porous media

8. The governing equations for the motion of a fluid are expressed as a system of differential equations. These equations satisfy the three basic physical conditions: continuity, rheological equation of state, and Newton's laws of motion. Together with a set of initial and boundary conditions, these equations completely define a given problem. The best known of these equations are those of Navier and Stokes[2] and are applicable to incompressible viscous fluids. The Navier-Stokes equations may be expressed as follows:[3]

$$X - \frac{1}{\rho}\frac{\partial p}{\partial x} + \frac{\nu}{3}\frac{\partial}{\partial x}\left(\frac{\partial u}{\partial x} + \frac{\partial v}{\partial y} + \frac{\partial w}{\partial z}\right) + \nu\nabla^2 u = \frac{Du}{\partial t} \tag{1a}$$

$$Y - \frac{1}{\rho}\frac{\partial p}{\partial y} + \frac{\nu}{3}\frac{\partial}{\partial y}\left(\frac{\partial u}{\partial x} + \frac{\partial v}{\partial y} + \frac{\partial w}{\partial z}\right) + \nu\nabla^2 v = \frac{Dv}{\partial t} \tag{1b}$$

$$Z - \frac{1}{\rho}\frac{\partial p}{\partial z} + \frac{\nu}{3}\frac{\partial}{\partial z}\left(\frac{\partial u}{\partial x} + \frac{\partial v}{\partial y} + \frac{\partial w}{\partial z}\right) + \nu\nabla^2 w = \frac{Dw}{\partial t} \tag{1c}$$

where

x,y,z = spatial coordinates

u,v,w = velocity components in x, y, and z directions

X,Y,Z = body forces in x, y, and z directions

$\rho = \gamma/g$, mass density of fluid

$\nu = \mu/\rho$, kinematic viscosity

$$\nabla^2 = \frac{\partial^2}{\partial x^2} + \frac{\partial^2}{\partial y^2} + \frac{\partial^2}{\partial z^2}$$

$$\frac{D}{\partial t} = \frac{\partial}{\partial t} + u\frac{\partial}{\partial x} + v\frac{\partial}{\partial y} + w\frac{\partial}{\partial z}$$

Application to viscous flow model

9. Hele-Shaw[4,5] developed the first parallel plate viscous flow model. It consists of two closely spaced, parallel plates (fig. 1). The

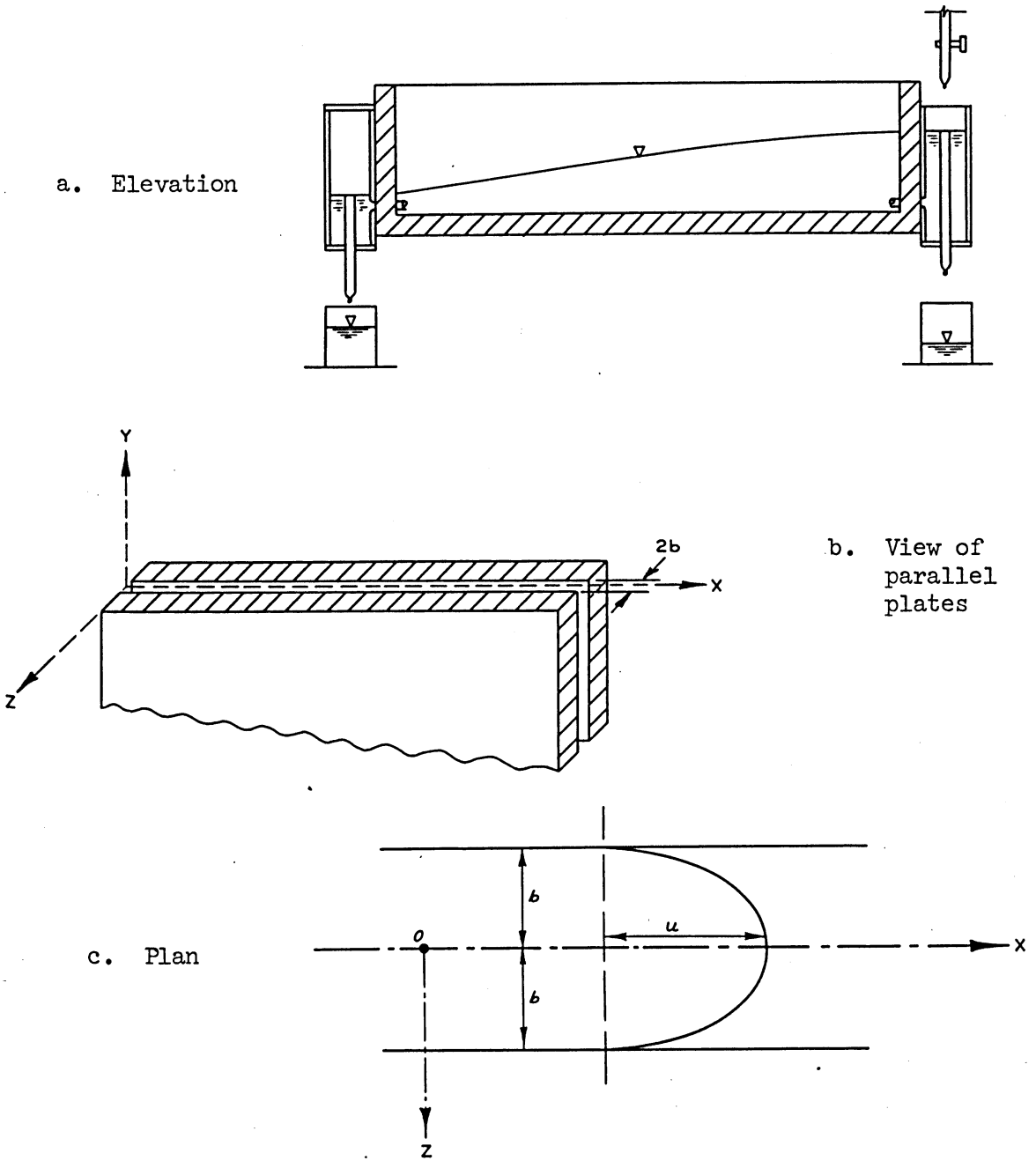

Fig. 1. Parallel plate model

narrow gap between the plates forms a channel through which the fluid flows. The channel represents a two-dimensional cross section of an unconfined homogeneous and isotropic aquifer. A regulating reservoir is provided at each end of the model. A regulating reservoir may be considered

as any body of open water that the aquifer intersects. One of the major advantages of the Hele-Shaw model is its clearly defined free surface, which eliminates the broad capillary zone of partial saturation that complicates the use of sand models.[6]

10. A sketch of the parallel plate model is shown in fig. 1. If the distance $2b$ between the two plates is small, the flow between the plates can be considered two-dimensional, with coordinate axes shown in fig. 1, and the velocity component w can be assumed zero. The gravitational forces are the only body forces acting on the system. The gravitational force can be replaced by a potential $\Omega = gH$, where H is the elevation head. Thus,

$$X = -\frac{\partial}{\partial x}(gH) \tag{2a}$$

$$Y = -\frac{\partial}{\partial y}(gH) \tag{2b}$$

$$Z = -\frac{\partial}{\partial z}(gH) \tag{2c}$$

11. For an incompressible fluid, there is no volume change, and hence the third term in equation 1 representing the rate of volume dilation can be ignored. Assuming the flow to be laminar, the fluid velocities at the plates must be zero (fig. 1b); hence the change in the velocity components u and v with respect to z will be much greater than the changes with respect to the x and y directions. Therefore, the derivatives $\frac{\partial u}{\partial x}$, $\frac{\partial u}{\partial y}$, $\frac{\partial v}{\partial x}$, and $\frac{\partial v}{\partial y}$ and also their second derivatives can be neglected.

12. Introducing the above assumptions in equation 1 yields

$$\frac{\partial}{\partial x}(\rho gH + p) - \mu \frac{\partial^2 u}{\partial z^2} = -\rho \frac{\partial u}{\partial t} \tag{3a}$$

$$\frac{\partial}{\partial y}(\rho gH + p) - \mu \frac{\partial^2 u}{\partial z^2} = -\rho \frac{\partial v}{\partial t} \tag{3b}$$

$$\frac{\partial}{\partial z}(\rho gH + p) = 0 \tag{3c}$$

For the special case of steady state flow, equation 3 will reduce to

$$\frac{\partial}{\partial x}(\rho g H + p) - \mu \frac{\partial^2 u}{\partial z^2} = 0 \tag{4a}$$

$$\frac{\partial}{\partial y}(\rho g H + p) - \mu \frac{\partial^2 v}{\partial z^2} = 0 \tag{4b}$$

$$\frac{\partial}{\partial z}(\rho g H + p) = 0 \tag{4c}$$

13. Equation 4c shows that the total head at any point within the flow domain will depend upon the x and y coordinates only. Hence, equations 4a and 4b can be integrated with respect to z to yield

$$z \frac{\partial}{\partial x}(\rho g H + p) = \mu \frac{\partial u}{\partial z} + c_1 \tag{5a}$$

and

$$z \frac{\partial}{\partial y}(\rho g H + p) = \mu \frac{\partial v}{\partial z} + c_2 \tag{5b}$$

Now, $\frac{\partial u}{\partial z} = \frac{\partial v}{\partial z} = 0$ when $z = 0$; therefore, from equation 5, we get

$$c_1 = c_2 = 0$$

Integrating once again with respect to z yields

$$\frac{z^2}{2} \frac{\partial}{\partial x}(\rho g H + p) = \mu u + c_3 \tag{6a}$$

and

$$\frac{z^2}{2} \frac{\partial}{\partial y}(\rho g H + p) = \mu v + c_4 \tag{6b}$$

Here $u = v = 0$ when $z = \pm b$; therefore,

$$c_3 = \frac{b^2}{2} \frac{\partial}{\partial x}(\rho g H + p)$$

and

$$c_4 = \frac{b^2}{2} \frac{\partial}{\partial y}(\rho g H + p)$$

$$u = \frac{z^2 - b^2}{2\mu} \frac{\partial}{\partial x} (\rho g H + p) \tag{6c}$$

$$v = \frac{z^2 - b^2}{2\mu} \frac{\partial}{\partial y} (\rho g H + p) \tag{6d}$$

14. Equation 6 shows that the distribution of velocity components is parabolic. The maximum velocity at the center of the gap, i.e., at $z = 0$, is

$$u = -\frac{b^2}{2\mu} \frac{\partial}{\partial x} (\rho g H + p) \tag{7a}$$

$$v = -\frac{b^2}{2\mu} \frac{\partial}{\partial y} (\rho g H + p) \tag{7b}$$

and the mean velocity is two-thirds of the maximum so that

$$\bar{u} = -\frac{b^2}{3\mu} \frac{\partial}{\partial x} (\rho g H + p) \tag{8a}$$

$$\bar{v} = -\frac{b^2}{3\mu} \frac{\partial}{\partial y} (\rho g H + p) \tag{8b}$$

Multiplying and dividing by ρg on the right-hand side and substituting $h = H + \frac{p}{\rho g}$ yields

$$\bar{u} = -\frac{b^2 \rho g}{3\mu} \frac{\partial h}{\partial x} \tag{9a1}$$

$$\bar{v} = -\frac{b^2 \rho g}{3\mu} \frac{\partial h}{\partial y} \tag{9a2}$$

$$\bar{u} = -m \frac{\partial h}{\partial x} \tag{9b1}$$

or

$$\bar{v} = -m \frac{\partial h}{\partial y} \tag{9b2}$$

where m designates the coefficient of permeability of the gap.

Description of Model

15. The viscous flow model consists of two parallel glass plates

0.5 in.* thick and rests on an adjustable I-beam that is supported on two columns. The glass plates are 11 ft long and 20 in. in height and rest on a plastic base plate that sits on the I-beam. Two plastic plates, each 0.25 in. thick, are inserted between the glass plates so that a desired width of gap between them is obtained. The plastic plates can be shaped to simulate any desired prototype configuration. A reservoir, approximately 8 sq in. in area, is provided at each end of the glass plates. Each reservoir is provided with a means for controlling the level of liquid in the reservoir. A view of the model is shown in fig. 2.

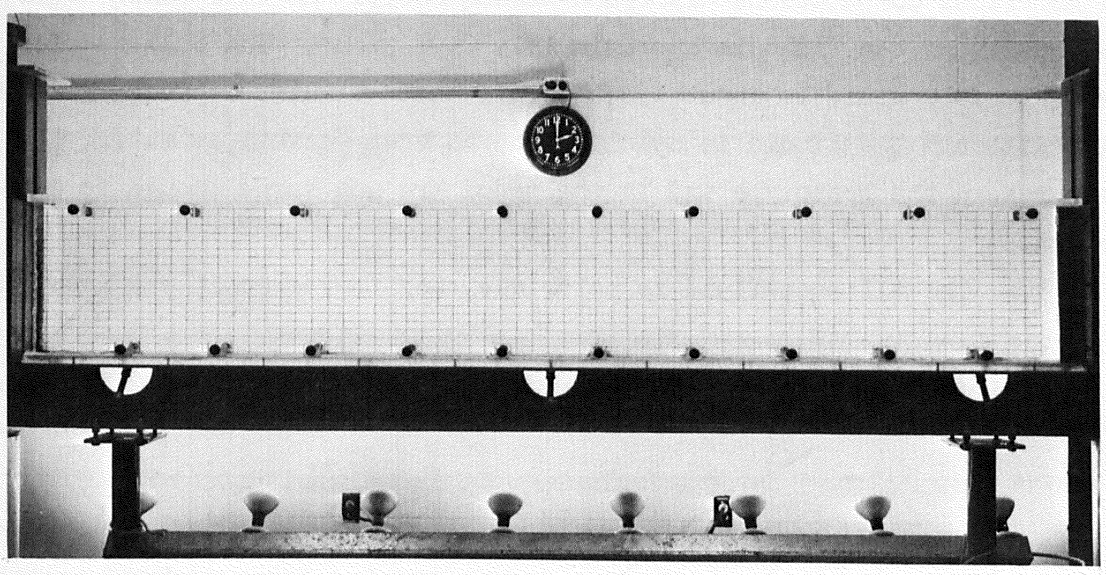

Fig. 2. View of model

Fluid used in model

16. The fluid used for the experiments is Silicone SF-96-1000, manufactured by General Electric Co. The following properties of the fluid are given by the manufacturer.

> Silicone fluid is chemically inert to most common materials of construction, and its density and viscosity do not change appreciably with temperature. The fluid has excellent stability under very high temperatures for long periods of time. It is self-extinguishing with flash point above 550 F and autoignition temperature in the range of 820 to 860 F. It has low surface tension,

* A table of factors for converting British units of measurement to metric units is presented on page xiii.

which is largely independent of viscosity (about 21 dynes per cm at 25 C, over a viscosity range of 20 to 100,000 centistokes). The thermal conductivity of the Silicone fluid is relatively constant over a wide range of temperature.

17. The number "1000" in the designation of the fluid stands for the nominal viscosity of 1000 centistokes. The actual viscosity-temperature relation was determined at WES; results are shown in fig. 3. The density-temperature relation is shown in fig. 4. At a temperature of 22 C, the viscosity of the Silicone fluid is about 9.7 stokes, and this value is used for numerical computations described subsequently. At this temperature, the density of the fluid is approximately 0.97 g/cm^3. The bulk modulus of the SF-96-1000 fluid is about 150,000 psi; that of water is about 300,000 psi. Although the liquid is nearly twice as compressible as water, the pressures in the prototype and in the model are not large enough to cause concern.

18. The Silicone fluid is colorless, and therefore it was necessary

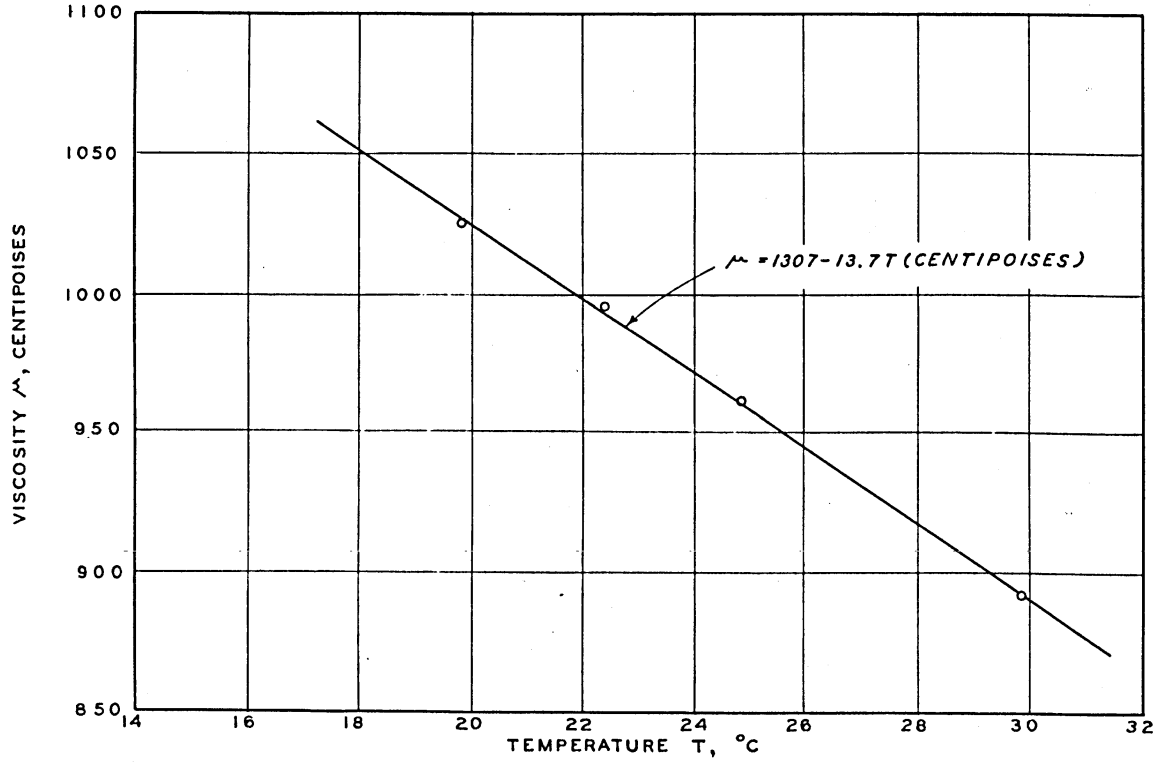

Fig. 3. Viscosity-temperature relation for Silicone SF-96-1000 fluid

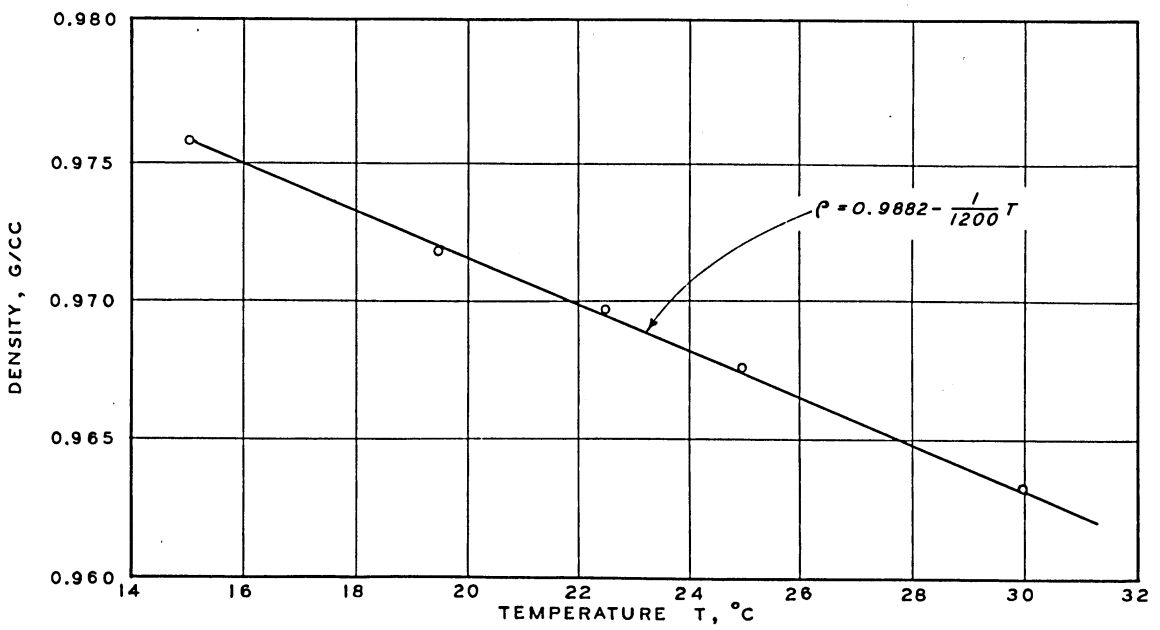

Fig. 4. Density-temperature relation for Silicone SF-96-1000 fluid

to add a coloring agent to it in order to obtain a distinct and clear free surface. The coloring material was Sudan Red 4BA supplied by General Dyestaff Co., New York.

19. Randolph Pump Model 500, manufactured by Randolph Co., Houston, Tex., was installed to pump the liquid into the reservoir.

Relation between model and prototype

20. Darcy's law representing a linear dependence between the hydraulic gradient and the discharge velocity is given by

$$v = -k \frac{\partial h}{\partial s} \tag{10a}$$

Using the relation between the permeability and the coefficient of permeability[3]

$$k = k_o \frac{\rho g}{\mu} \tag{10b}$$

equation 10a is transformed to

$$v = -\frac{k_o \rho g}{\mu} \frac{\partial h}{\partial s} \tag{10c}$$

where

k = coefficient of permeability, L/T

k_o = permeability, L^2

s = coordinate direction along the stream line

21. Now, writing equation 9 for the model and equation 10c for the prototype yields

$$V_m = V_{model} = -\frac{b^2 \rho_m g}{3\mu_m} \frac{\partial h}{\partial s} \tag{11a}$$

and

$$V_p = V_{prototype} = -\frac{k_o \rho_p g}{\mu_p} \frac{\partial h}{\partial s} \tag{11b}$$

22. The velocity ratio between the model and prototype, for the same gradients, is given by

$$V_r = \frac{V_m}{V_p} = \frac{b^2}{3} \frac{\rho_r}{k_o \mu_r}$$

$$= \frac{b^2 \rho_m g}{3k\mu_m} \tag{12}$$

Selection of model scales

23. The properties of the Silicone fluid, SF-96-1000, at 26 C are given by

$$\rho_m = 0.967 \text{ g/cm}^3$$

$$\mu_m = 9.7 \text{ poises}$$

Therefore

$$V_r = \frac{0.967 \times 980}{3 \times 9.7} \cdot \frac{b^2}{k}$$

$$= 33.0 \frac{b^2}{k} \tag{13}$$

Now

$$V_r = \frac{L_r}{T_r}$$

where L_r = length scale ratio and T_r = time scale ratio. Sample calculations for model dimensions are given below for certain numerical values of prototype conditions.

a. For a flood of 75 ft, simulated by 1.25 ft in the model,

$$L_r = \frac{1.25}{75} = 0.0167$$

b. For a flood of 1 week (≃605,000 sec), simulated in the model by approximately 8 min (480 sec),

$$T_r = \frac{480}{605,000} = \frac{1}{1260}$$

Therefore

$$V_r = \frac{0.0167}{1/1260} = 21.00 \qquad (14)$$

c. Equating equations 13 and 14 yields

$$33 \frac{b^2}{k} = 21$$

where

b = half width, cm

k = permeability, cm/sec

or

$$b^2 = 0.635k$$

If

$$k = 100 \times 10^{-4} \text{ cm/sec}$$

$$b^2 = 0.635 \times 100 \times 10^{-4}$$

and

$$b = 0.08 \text{ cm}$$

and the width $w = 2 \times b = 0.16$ cm or approximately 1/16 in.

24. Values of T_r for different combinations of b and k are given below.

w	b	k , cm/sec	$T_r = \frac{0.0167}{33} \frac{k}{b^2}$
1/8 in.	1/16 in. (0.16 cm)	100×10^{-4}	1/5000
		500×10^{-4}	1/1000
		1000×10^{-4}	1/500
1/16 in.	1/32 in. (0.08 cm)	100×10^{-4}	1/1250
		500×10^{-4}	1/250
		1000×10^{-4}	1/125

For a given L_r, the following relation can be written

$$33 \frac{b^2}{k} = \frac{0.0167}{T_r} \tag{15}$$

PART III: CLOSED FORM SOLUTIONS

One-Dimensional Flow

Governing equation

25. The differential equation governing unconfined flow in one direction can be derived by using equation 9a.

$$\bar{u} = -\frac{b^2 \rho g}{3\mu} \frac{\partial h}{\partial x} \qquad \text{(9a1 bis)}$$

The continuity equation can be derived by considering the flow through the faces of a small element, fig. 5.

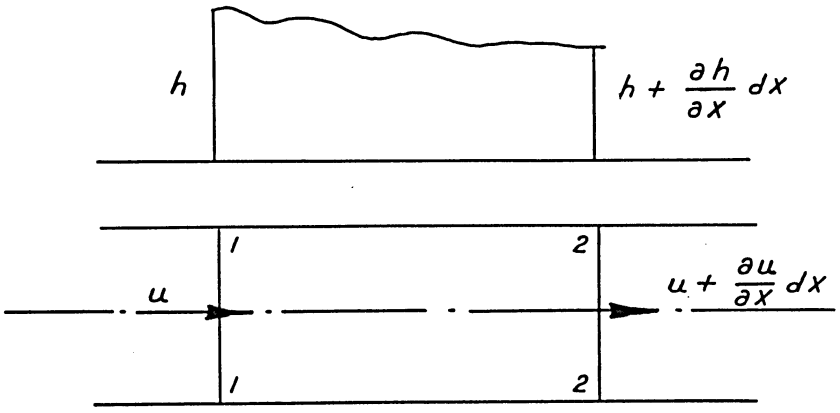

Fig. 5. Flow in an element of fluid

a. The flow through the face 1-1 is given as

$$q_{n1} = 2bhu \qquad \text{(16a)}$$

b. The flow through the face 2-2 is given by

$$q_{n2} = 2b\left(h + \frac{\partial h}{\partial x} dx\right)\left(u + \frac{\partial u}{\partial x} \cdot dx\right) \qquad \text{(16b)}$$

c. The change in flow between the faces 1-1 and 2-2 is given by

$$q_{n1} - q_{n2} = 2bhu - \left(2bhu + 2bh \frac{\partial u}{\partial x} dx + 2bu \frac{\partial h}{\partial x} dx\right) + 2b \frac{\partial h}{\partial x} \frac{\partial u}{\partial x} (dx)^2 \qquad \text{(16c)}$$

d. The last term, being of higher order, is neglected; thus

$$q_{n1} - q_{n2} = 2bh \frac{\partial u}{\partial x} dx - 2bu \frac{\partial h}{\partial x} dx \qquad (16d)$$

e. Assuming the fluid to be incompressible, the change in the flow must also be equal to $2b \cdot dx \cdot n \cdot \frac{\partial h}{\partial t}$, where n is the effective porosity and is equal to 1 for the slit in the model. Then the complete flow equation becomes

$$-2bh \frac{\partial u}{\partial x} dx - 2bu \frac{\partial h}{\partial x} dx = 2b\, dx\, n \frac{\partial h}{\partial t} \qquad (17)$$

Substituting the value of $\frac{\partial u}{\partial x}$ from equation 9 yields

$$-2bh\left(-\frac{b^2}{3} \frac{\rho g}{\mu} \frac{\partial^2 h}{\partial x^2}\right) dx - 2b\left(-\frac{b^2 \rho g}{3\mu} \frac{\partial h}{\partial x}\right) \frac{\partial h}{\partial x} dx = n \cdot 2b \cdot dx \frac{\partial h}{\partial t} \qquad (18)$$

Simplifying equation 18 gives

$$\frac{b^2 \rho g}{3\mu n}\left[h \frac{\partial^2 h}{\partial x^2} + \left(\frac{\partial h}{\partial x}\right)^2\right] = \frac{\partial h}{\partial t} \qquad (19)$$

26. Equation 19 is the governing differential equation for unconfined flow through the Hele-Shaw model. It also represents flow through porous media when the term $\frac{b^2 \rho g}{3\mu n}$ is replaced by $\frac{k_o \rho g}{\mu n}$, where k_o is the permeability of soil. Equation 19 is a nonlinear partial differential equation. If the change in head h is small compared with the height of the aquifer, the term $\left(\frac{\partial h}{\partial x}\right)^2$ can be neglected and $h \frac{\partial^2 h}{\partial x^2}$ can be replaced by $\bar{h} \frac{\partial^2 h}{\partial x^2}$, where $\bar{h}$ is either the original depth of water in the aquifer or the mean height in the case of a rising river level.

27. Thus the nonlinear equation is reduced to linear partial differential equation:

$$\frac{b^2 \rho g}{3\mu n} \bar{h} \frac{\partial^2 h}{\partial x^2} = \frac{\partial h}{\partial t} \tag{19a}$$

or

$$\frac{\partial h}{\partial t} = \alpha \frac{\partial^2 h}{\partial x^2} \tag{19b}$$

where $\alpha = \frac{b^2 \rho g}{3\mu n} \bar{h}$.

Closed form solutions

28. Linearized equation. Several closed form solutions are available for the governing differential equation 19 with simple boundary conditions. Since numerical solutions are used in this study, only a brief review of such closed form solutions will be presented here.

29. Rise of flood at constant rate. Carslaw and Jaeger[7] and Hantush[8] have derived the solution of equation 19 for the following simple boundary conditions and a bank with vertical upstream face.

Boundary conditions:

$$h(x,o) = 0$$

$$h(\infty,o) = 0$$

$$h(o,t) = ct$$

where

$h(x,t)$ = head at distance x occurring at time t

x = distance from upstream face

t = time

c = rate of rise of head at upstream face

30. The solution to equation 19 with the above boundary conditions is given in references 7 and 8.

$$h(x,t) = ct\left[(1 + 2U^2)\ \text{erfc}\ (U) - \frac{2}{\sqrt{\pi}} U \exp\ (-U^2)\right] \tag{20a}$$

where $U = \frac{x}{\sqrt{4\alpha t}}$.

31. The solution for the case when the flood rises at a constant

rate up to a certain head and remains steady is also obtained (equation 20b) by superposition of two linear functions, as shown in fig. 6.[7]

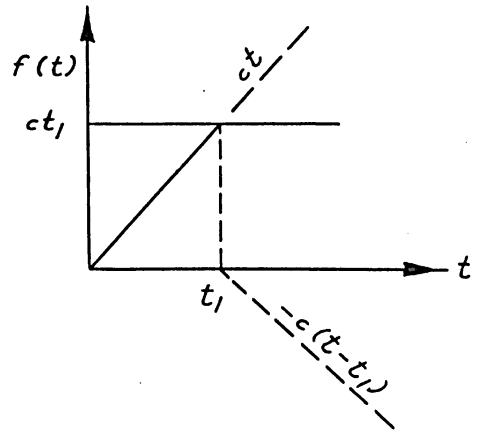

Fig. 6. Superposition of two linear functions

$h(x,t)$ = same as in equation 20a for $0 \le t \le t_1$

$$h(x,t) = ct\left[(1 + 2U^2)\ \text{erfc}\ (U) - \frac{2}{\sqrt{\pi}} U \exp(-U^2)\right] - c(t - t_1)\left[\left(1 + 2U_1^2\right)\text{erfc}\ (U_1) - \frac{2}{\sqrt{\pi}} U_1 \exp\left(-U_1^2\right)\right] \quad \text{for } t \ge t_1 \tag{20b}$$

where $U_1 = \dfrac{x}{\sqrt{4\alpha(t - t_1)}}$.

32. Sinusoidal rise of flood. Cooper and Rorabaugh[9] obtained the solution to equation 19 with sinusoidal rise of flood and the following boundary conditions.

Boundary conditions:

$$h(x,o) = 0 \qquad x \ge 0$$

$$h(\infty,t) = 0 \qquad t \ge 0$$

$$h(0,t) = \begin{cases} \dfrac{h_o}{2}(1 - \cos \omega t) & t \le T \\ 0 & t \ge T \end{cases}$$

where

ω = frequency of flood

T = period of flood

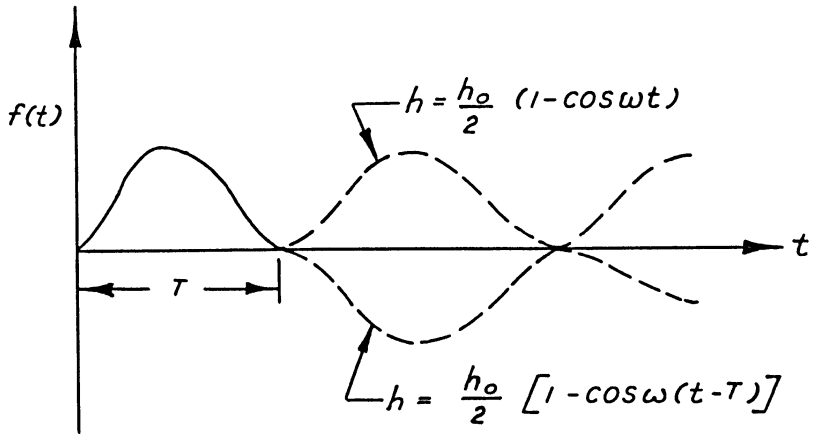

Fig. 7. Superposition of waves

33. The solution for the case of rise and fall of flood (fig. 7) up to time T and then steady conditions is obtained by superposition of sine waves, as shown in fig. 7.[9]

$$h(x,t) = \frac{h_o}{2}\left\{\operatorname{erfc}\frac{x}{2\sqrt{\alpha t}} - \operatorname{erfc}\left[\frac{x}{2\sqrt{\alpha(t-T)}}\right]\right\}$$

$$+ \frac{1}{\pi}\int_0^\infty \left[e^{-Ut} - e^{-U(t-T)}\right] \sin\left(x\sqrt{U/\alpha}\right) \frac{U}{U^2+\omega^2}\, dU \qquad (21)$$

34. Nonlinear equation. The results of the linearized equation are applicable only to the cases where the height of flood is small compared to the original aquifer depth. In cases where the height of flow is not small compared to the depth of aquifer, the above results are not applicable and the nonlinear differential equation should be considered.

35. Exponential rate of flood rise. Polubarinova-Kochina[10] has obtained a solution to the nonlinear equation 19 and the following boundary conditions.

Nonlinear equation:

$$\frac{\partial h}{\partial t} = \alpha_1 \left[\left(\frac{\partial h}{\partial x} \right)^2 + h \frac{\partial^2 h}{\partial x^2} \right] \tag{19}$$

where $\alpha_1 = \frac{b^2 \rho_m g}{3 \mu_m n}$ or

$$\frac{\partial h}{\partial t} = \lambda^2 \frac{\partial^2 (h^2)}{\partial x^2} \tag{22}$$

where $\lambda^2 = \frac{\alpha_1}{2}$.

Boundary conditions:

$$h(x,o) = 0$$

$$h(o,t) = ct^p \qquad p > 0$$

36. The equation is solved by assuming the solution in the following form.

$$h(x,t) = ct^p f(\psi) \tag{23}$$

where $\psi = \frac{x}{\lambda \sqrt{c^{k-1} t^{[1+p(k-1)]}}}$. For the special case of $p = 1$, giving linear rate of flood rise, the solution is presented in reference 10 as

$$h = ct - x\sqrt{\frac{c}{2\lambda^2}} \qquad \text{for} \quad 0 \le x \le \sqrt{2\lambda^2 c}\, t$$

$$h = 0 \qquad \text{for} \quad x > t\sqrt{2\lambda^2 c} \tag{24}$$

Equation 24 shows that $\frac{dx}{dt} = \sqrt{2\lambda^2 c}$ and indicates that the water front travels with a constant velocity equal to $\sqrt{2\lambda^2 c}$.

Two-Dimensional Flow

Governing equation

37. The governing differential equation for two-dimensional flow can

be obtained by using a procedure similar to that in paragraph 25. An approximate derivation is shown in Appendix A according to which a special nonlinear form of the equation is

$$\frac{\partial h}{\partial t} = \frac{k_x}{n} \frac{\partial}{\partial x}\left(h \frac{\partial h}{\partial x}\right) + \frac{k_y}{n} h \frac{\partial^2 h}{\partial y^2} \tag{25}$$

where

k_x and k_y = permeabilities in x and y directions

n = porosity

Solution by linearization

38. It is difficult to obtain a closed form solution to equation 25 in the nonlinear form. Brahma and Harr[11] modified equation 25 to a linearized form

$$\frac{\partial h}{\partial t} = \frac{k\bar{h}}{n}\left(\frac{\partial^2 h}{\partial x^2} + \frac{\partial^2 h}{\partial y^2}\right) \tag{26}$$

where

$\bar{h}$ = mean upstream head

k = uniform permeability

and obtained solutions by expressing equation 26 in polar coordinates r,θ (fig. 8).

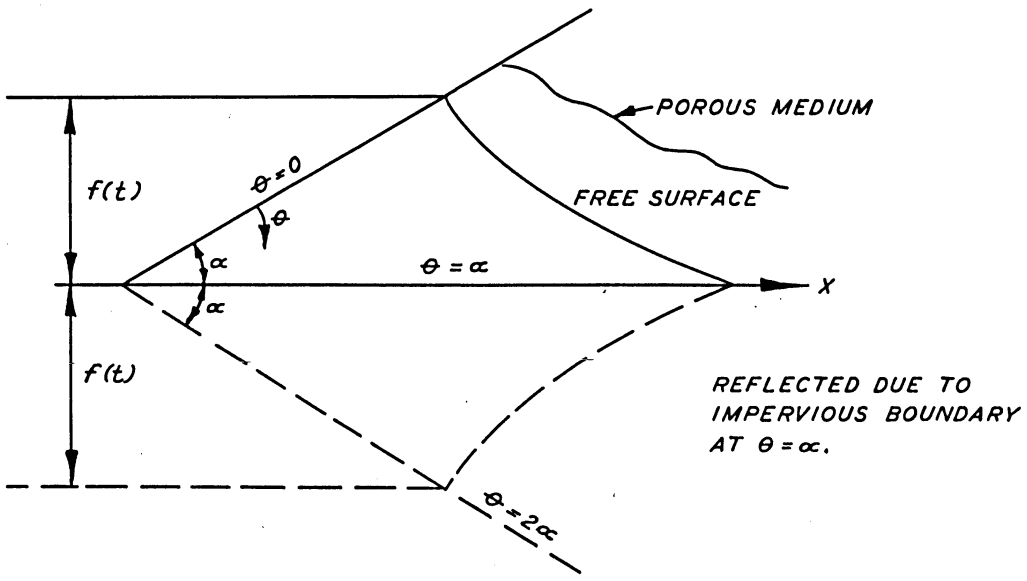

Fig. 8. Section of a porous boundary to account for impervious boundary[11]

$$\frac{\partial h}{\partial t} = \frac{k\bar{h}}{n}\left(\frac{\partial^2 h}{\partial r^2} + \frac{1}{r}\frac{\partial h}{\partial r} + \frac{1}{r^2}\frac{\partial^2 h}{\partial \theta^2}\right) \qquad (27)$$

with the following boundary conditions:

(i) $h(r,\theta,0) = 0$ for $r > 0$, $0 < \theta < 2\alpha$

(ii) $h(r,0,t) = h(r,2\alpha,t) = H$ or $= f(t)$

(iii) $h(r,\theta,t) = r \sin(\alpha - \theta)$ on free surface

where

H = instantaneous head

f(t) = function giving variation of flood

39. The solution for the case of instantaneous rise of head H is obtained as:

$$\frac{h(r,\theta,t)}{H} = 1 - \frac{2}{\alpha}\sum_{i=0}^{\infty} \sin s\theta \left\{\frac{\sqrt{\pi}}{4s\sqrt{\tau}}\left[\frac{I_{s-1}}{2}\left(\frac{1}{8\tau}\right) + \frac{I_{s+1}}{2}\left(\frac{1}{8\tau}\right)\right]\exp\left(-\frac{1}{8\tau}\right)\right\} \qquad (28)$$

where

$$s = \left(\frac{2i+1}{2}\right)\frac{\pi}{\alpha}$$

$$\tau = \frac{kt}{r^2}$$

$$k = \frac{k\bar{h}}{n}$$

I = modified Bessel function

The solution for linear rise of flood is:

$$\frac{h(r,\theta,t)}{ct} = 1 - \frac{2}{\alpha\tau}\sum_{i=0}^{\infty} \sin s\theta \int_0^{\infty}\left(1 - e^{-\tau u^2}\right)\frac{J_s(u)}{u^3}\,du \qquad (29)$$

where $J_s(u)$ is the Bessel function. For further details on the derivation of equations 28 and 29, refer to the paper by Brahma and Harr.[11] The free surface is determined from the solutions of equations 28 and 29, such that boundary condition iii is satisfied.

PART IV: NUMERICAL SOLUTIONS

40. The basic differential equation governing unsteady flow of liquids through porous media is nonlinear, and no closed form solutions are readily available for arbitrary boundary and initial conditions. Even a linearized form of the equation is difficult to solve in closed form for arbitrary and variable boundary conditions. It is intended, therefore, to develop approximate numerical solutions for the one-dimensional linearized and nonlinear equations and for linearized and nonlinear two-dimensional equations. With the availability of high-speed computers and some stable and efficient numerical schemes, it is possible to obtain satisfactory solutions by using numerical techniques.

41. In this part of the report, the equations governing the flow of fluid are shown in the form of difference equations using the finite difference technique. In Part VI, the finite element method is used to solve the complete problem of transient flow through porous media.

One-Dimensional Flow

Linearized equation

42. The linearized equation governing one-dimensional flow is given by equation 19b:

$$\frac{\partial h}{\partial t} = \frac{b^2 \rho g}{3\mu n} \frac{\bar{h}}{h} \frac{\partial^2 h}{\partial x^2}$$

$$= \alpha \frac{\partial^2 h}{\partial x^2} \qquad \text{(19b bis)}$$

Adopting a grid scheme such as that shown in fig. 9, an approximate central finite difference representation[12] for $\frac{\partial^2 h}{\partial x^2}$ is given by

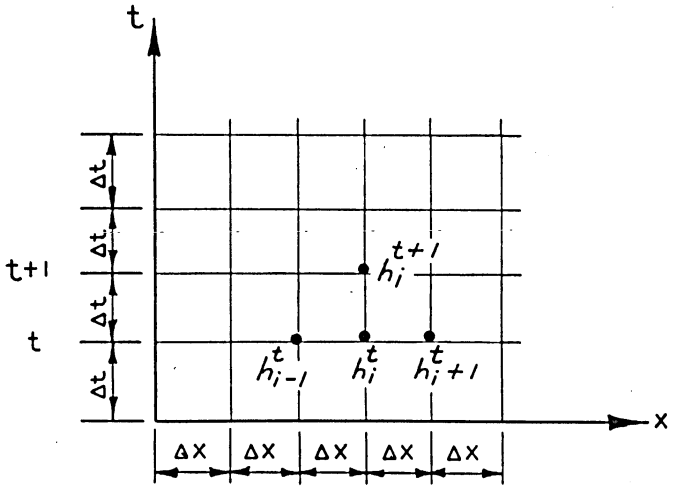

Fig. 9. Finite difference approximation

$$\frac{\partial^2 h}{\partial x^2} = \frac{h_{i-1}^t - 2h_i^t + h_{i+1}^t}{(\Delta x)^2} \tag{30a}$$

and for $\frac{\partial h}{\partial t}$,

$$\frac{\partial h}{\partial t} = \frac{h_i^{t+1} - h_i^t}{\Delta t} \tag{30b}$$

where Δx and Δt are finite intervals in the x and t directions, respectively. Equation 19b can now be expressed as:

$$\frac{h_i^{t+1} - h_i^t}{\Delta t} = \frac{\alpha}{(\Delta x)^2}\left(h_{i-1}^t - 2h_i^t + h_{i+1}^t\right)$$

or

$$h_i^{t+1} = \frac{\alpha \Delta t}{(\Delta x)^2}\left(h_{i-1}^t - 2h_i^t + h_{i+1}^t\right) + h_i^t \tag{30c}$$

Equation 30c is computationally stable for

$$\frac{\alpha \Delta t}{(\Delta x)^2} \leq \frac{1}{2}$$

43. The magnitudes of head h at a time $t + \Delta t$ can be computed by using equation 30c, since all other quantities are known from the initial and boundary conditions described below.

Boundary conditions

44. At time $t = 0$ for a dry bank, zero head may be specified at all points within the bank, or alternatively, any initial head distribution may be assumed. Also, any head variation at the upstream face of the bank may be specified. The cases of constant rate of rise or fall of flood, sudden drawdown case, and sinusoidal rate of flood are considered in this study. Head outside the downstream face is assumed equal to zero for all times.

Alternative linearization

45. The linearization in equation 19 essentially yields solutions of the form

$$h(x,t) = c_1 x + c_2 \tag{31}$$

where c_1 and c_2 are constants. Equation 31 is a linear function and indicates that the equation of the free surface of flow is obtained in the form of a straight line given by equation 31.[10] This is suitable only for $c_1 = 0$, and for larger values of downstream head compared to the net effective head.

46. The expression in equation 19 can be linearized by adopting h^2 as the unknown function,[10] which gives parabolic function for the free surface. Replacing h^2 by u yields

$$\frac{\partial u}{\partial t} = \alpha_1 \sqrt{u} \frac{\partial^2 u}{\partial x^2} \tag{32}$$

where $\sqrt{u}$ is mean height of the reservoir. A finite difference approximation for equation 32 may be expressed as:

$$u_i^{t+1} = u_i^t + \alpha_1 \sqrt{u} \left(u_{i-1}^t - 2u_i^t + u_{i+1}^t \right) \tag{33}$$

where $u_i = h_i^2$.

Nonlinear equation

47. The nonlinear equation 19 can be rewritten as:

$$\frac{\partial h}{\partial t} = \frac{b^2 \rho g}{3\mu n} \frac{1}{2} \frac{\partial^2 (h^2)}{\partial x^2} \tag{34a}$$

or

$$\frac{\partial h}{\partial t} = \alpha_2 \frac{\partial^2 (H)}{\partial x^2} \tag{34b}$$

where

$$\alpha_2 = \frac{b^2 \rho g}{6\mu n}$$

$$H = h^2$$

An explicit form of finite difference approximation to equation 34b is:[13]

$$h_i^{t+1} = h_i^t + \frac{\alpha_2 \Delta t}{(\Delta x)^2} \left(H_{i-1}^t - 2 \cdot H_i^t + H_{i+1}^t \right) \tag{35}$$

Equation 35 is computationally stable for

$$\frac{\alpha_2 \Delta t}{(\Delta x)^2} < \frac{1}{4\bar{h}}$$

where $\bar{h} = \frac{\left(h_i^t + h_i^{t+1}\right)}{2}$.

Computer solutions

48. Three computer programs, prepared corresponding to equations 30c, 33, and 35, are used to solve for different conditions of head distributions at the upstream face. The results are compared with experimental results from the viscous flow model and are presented in Part V.

Two-Dimensional Flow

Linearized equation

49. The linearized form of the equation governing two-dimensional flow is given by

$$\frac{\partial h}{\partial t} = \frac{\bar{h}}{n}\left(k_x \frac{\partial^2 h}{\partial x^2} + k_y \frac{\partial^2 h}{\partial y^2}\right) \tag{36}$$

Equation 36 is in a form similar to the equations for heat flow considered by Larkin.[14] Equation 36 may be cast in finite difference form such that head at time $t + \Delta t$ can be computed from heads at time t . But in such a procedure, the computational stability depends on the magnitudes of the space intervals Δx and Δy and the time interval Δt . This difficulty can be avoided by using the scheme called "Alternating Direction Explicit Procedure (ADEP)."[14] In ADEP, stable solutions are obtained for any size of space and time intervals.

50. The finite difference approximation for ADEP is derived as follows (fig. 10). Let

$$\Delta x_2 = \beta_x \Delta x_1$$

$$\Delta y_2 = \beta_y \Delta y_1$$

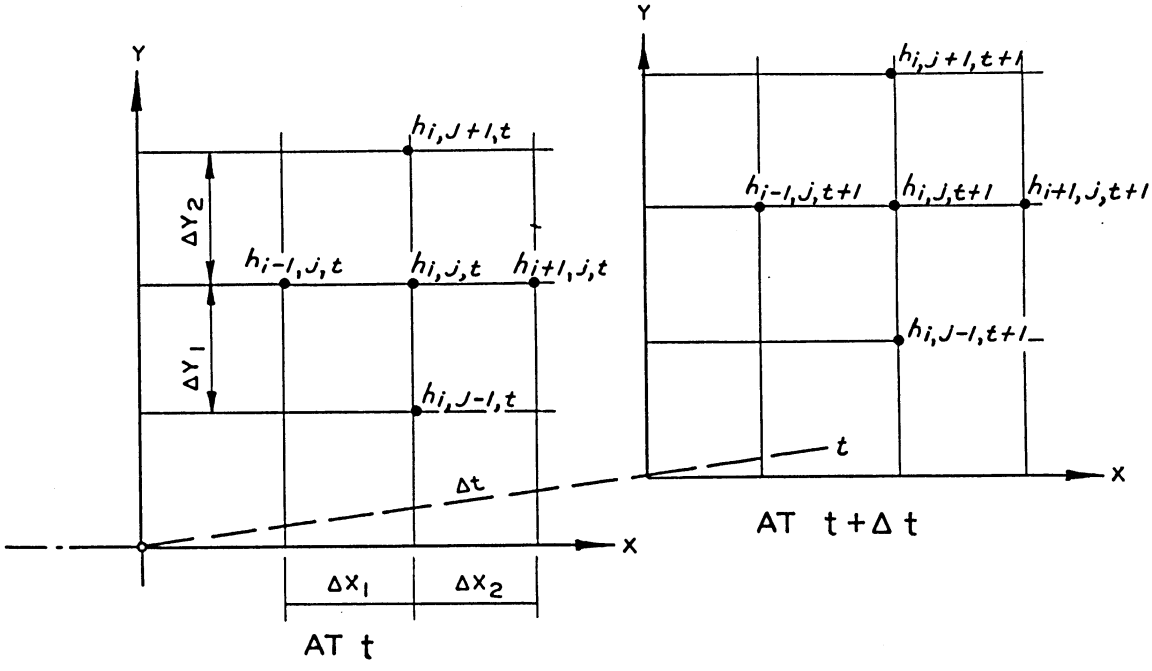

Fig. 10. Finite difference approximation for ADEP

$$\frac{\partial^2 h}{\partial x^2} = \frac{\dfrac{h_{i-1,j,t+1} - h_{i,j,t+1}}{\Delta x_1} - \dfrac{h_{i,j,t} - h_{i+1,j,t}}{\beta_x \Delta x_1}}{\frac{1}{2}\left(\Delta x_1 + \beta_x \Delta x_1\right)}$$

$$= \frac{2}{\Delta x_1^2 \left(1 + \beta_x\right)} \left(h_{i-1,j,t+1} - h_{i,j,t+1} - \frac{h_{i,j,t}}{\beta_x} + \frac{h_{i+1,j,t}}{\beta_x} \right) \quad (37a)$$

Similarly,

$$\frac{\partial^2 h}{\partial y^2} = \frac{2}{\Delta y_1^2 \left(1 + \beta_y\right)} \left(h_{i,j-1,t} - h_{i,j,t} - \frac{h_{i,j,t+1}}{\beta_y} + \frac{h_{i,j+1,t+1}}{\beta_y} \right) \quad (37b)$$

and

$$\frac{\partial h}{\partial t} = \frac{h_{i,j,t+1} - h_{i,j,t}}{\Delta t} \quad (37c)$$

Substituting 37a, 37b, and 37c into equation 36, we get

$$h_{i,j,t+1}\left(1 + A_x + \frac{A_y}{\beta_y}\right) = h_{i,j,t}\left(1 - \frac{A_x}{\beta_x} - A_y\right)$$

$$+ A_x\left(h_{i-1,j,t+1} + \frac{h_{i+1,j,t}}{\beta_x}\right) + A_y\left(h_{i,j-1,t} + \frac{h_{i,j+1,t+1}}{\beta_y}\right) \quad (38a)$$

or

$$h_{i,j,t+1} = \frac{c_x}{D} h_{i,j,t} + \frac{A_x}{D}\left(h_{i-1,j,t+1} + \frac{1}{\beta_x} h_{i+1,j,t}\right)$$

$$+ \frac{A_y}{D}\left(h_{i,j-1,t} + \frac{1}{\beta_y} h_{i,j+1,t+1}\right) \quad (38b)$$

where

$$A_x = \frac{2 \cdot k_x \bar{h} \cdot \Delta t}{n \cdot \Delta x_1^2 (1 + \beta_x)}$$

$$A_y = \frac{2 \cdot k_y \cdot \bar{h} \cdot \Delta t}{n \cdot \Delta y_1^2 (1 + \beta_y)}$$

$$c_x = 1 - \frac{A_x}{\beta_x} - A_y$$

$$D = 1 + A_x + \frac{A_y}{\beta_y}$$

For uniform grid, $\beta_x = \beta_y = 1$.

Boundary conditions

51. At $t = 0$:

(i) $h(x,y,0) = 0$ for an initially dry bank

(ii) $h(x, x \tan \alpha, t) = f(t)$

(iii) $\frac{\partial h}{\partial y} = 0$ at the impervious base

At free-water surface:

(iv) $h(x,y,t) =$ elevation head

52. The solution of equation 38b is obtained for the above boundary conditions and then the free surface is obtained by satisfying condition iv. A computer program has been prepared for equation 38b. The finite difference scheme was also used directly for the two-dimensional nonlinear equation 25. Details regarding this scheme and comparison of its results are presented in Part V.

Nonhomogeneous materials

53. It is possible to incorporate porous media with differing permeabilities in the finite difference scheme. The basic formulation for flow in nonhomogeneous media was based essentially on equation 25. However, at an interface between two materials with differing permeabilities, certain additional continuity conditions should be satisfied. Since the flow across an interface is constant, a relation between heads on either side of the interface can be obtained by equating the Darcy expressions for flow in the two materials. It was also necessary, as a numerical expedient, to establish a point in one of the materials as if the other material was extending into it, and define a fictitious head at that point.[12] Formulation based on these considerations is obtained and is given in Appendix B.

Drawdown conditions

54. The case of sudden and gradual drawdown is of importance for the stability of riverbanks. A numerical solution for one-dimensional flow was obtained for sinusoidal rise and fall of fluid (fig. 15, page 38). The drawdown conditions require special attention since, when drawdown occurs from a bank after a flood rises to a certain height and then recedes, the flow of fluid takes place toward both the upstream and downstream directions. Also, the soil medium above the falling free surface passes from one state of saturation to another. Consideration should also be given to the surface of seepage at the exiting faces. To account for the condition of partial saturation above the free surface, the basic equation can be expressed such that the left-hand side of equation 25 represents the time rate of change of moisture content in the soil. Then the finite difference scheme can be used for the solution of the modified equation and location of the free surface. Formulation for the two-dimensional flow is obtained for certain simple conditions, and work toward a general solution is in progress.

PART V: COMPARISON OF RESULTS

One-Dimensional Flow

Experimental results

55. An experiment (series C_4) was performed with the viscous flow model, adopting a plate length of 187 cm with vertical upstream face. The width of the gap between the parallel plates was determined experimentally from the measurements of flow of fluid under steady state conditions. Six such flow measurements were made and the average width of 0.10 cm was computed using the following equation.[6]

$$Q = \frac{b^3 \rho g}{3\mu L}\left(h_1^2 - h_2^2\right) \tag{39}$$

where

Q = flow

ρ = density of fluid = 0.97 g/cm^3

μ = viscosity of fluid = 9.7 g/cm-sec

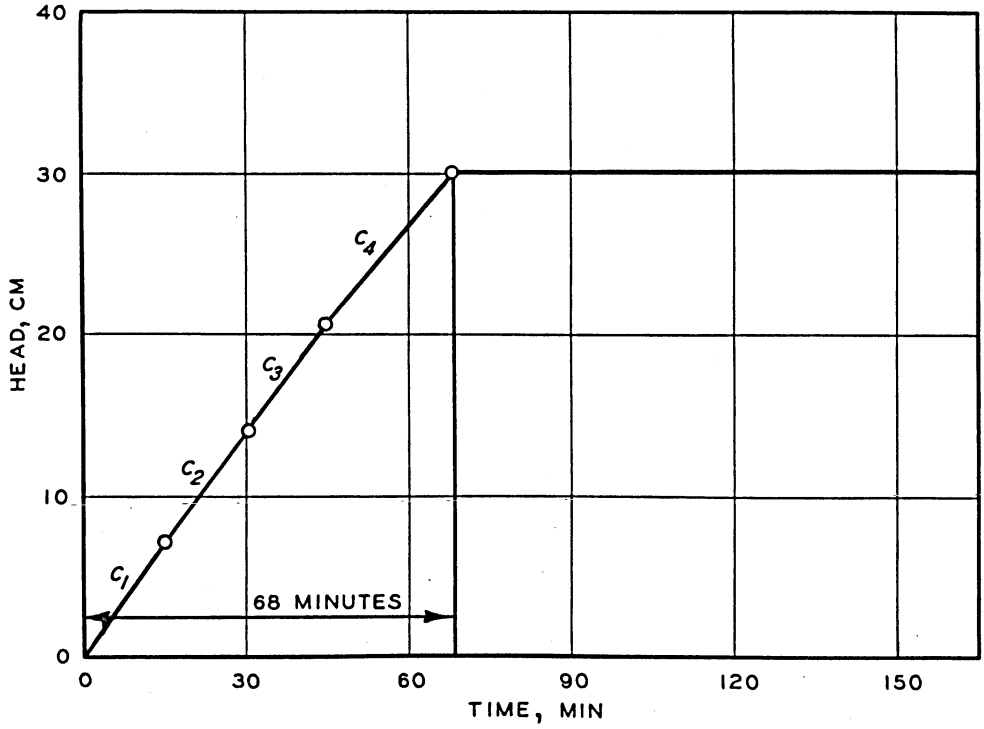

Fig. 11. Rise of river (Test C_4)

L = length of plates = 187 cm

g = gravitational constant = 980 cm/sec^2

h_1 = upstream steady state head

h_2 = downstream tailwater head (equal to zero for all tests presented in this report)

56. The liquid head in the reservoir was raised by pumping the liquid at a constant rate. The rate of rise of head in the reservoir was approximated by dividing the total time of rise into four parts and computing four separate linear rates of rise, fig. 11. The head was raised up to a height of 30 cm and was kept steady thereafter. Photographic records of the development of free surface in the model were obtained at certain selected time periods. Typical photographic observations are shown in fig. 12 for time periods of 15, 30, 60, and 75 min, respectively. The head distributions for these periods are plotted in fig. 13.

Numerical results

57. As mentioned in Part IV, computer programs have been prepared corresponding to equations 30c, 33, and 35 and are designated as LINI, LINII, and NONLIN, respectively. The free-surface heads are computed by employing these programs and incorporating the following parameters.

Fluid properties: density (ρ) = 0.97 g/cm^3
viscosity (μ) = 9.7 g/cm-sec

Model properties: width of gap (b) = 0.10 cm
length (L) = 187 cm
porosity (n) = 1.0
Δx = 9.35 cm
Δt = 2.5 sec
g = 980 cm/sec^2

Comparison

58. The results from numerical techniques are plotted in fig. 13 in comparison with the results from the experiments. The head distributions from numerical methods are found generally to lie above the experimental values. The discrepancy may be due to numerical approximations, defects in the model, experimental errors, leakage of fluid, friction at the base, and

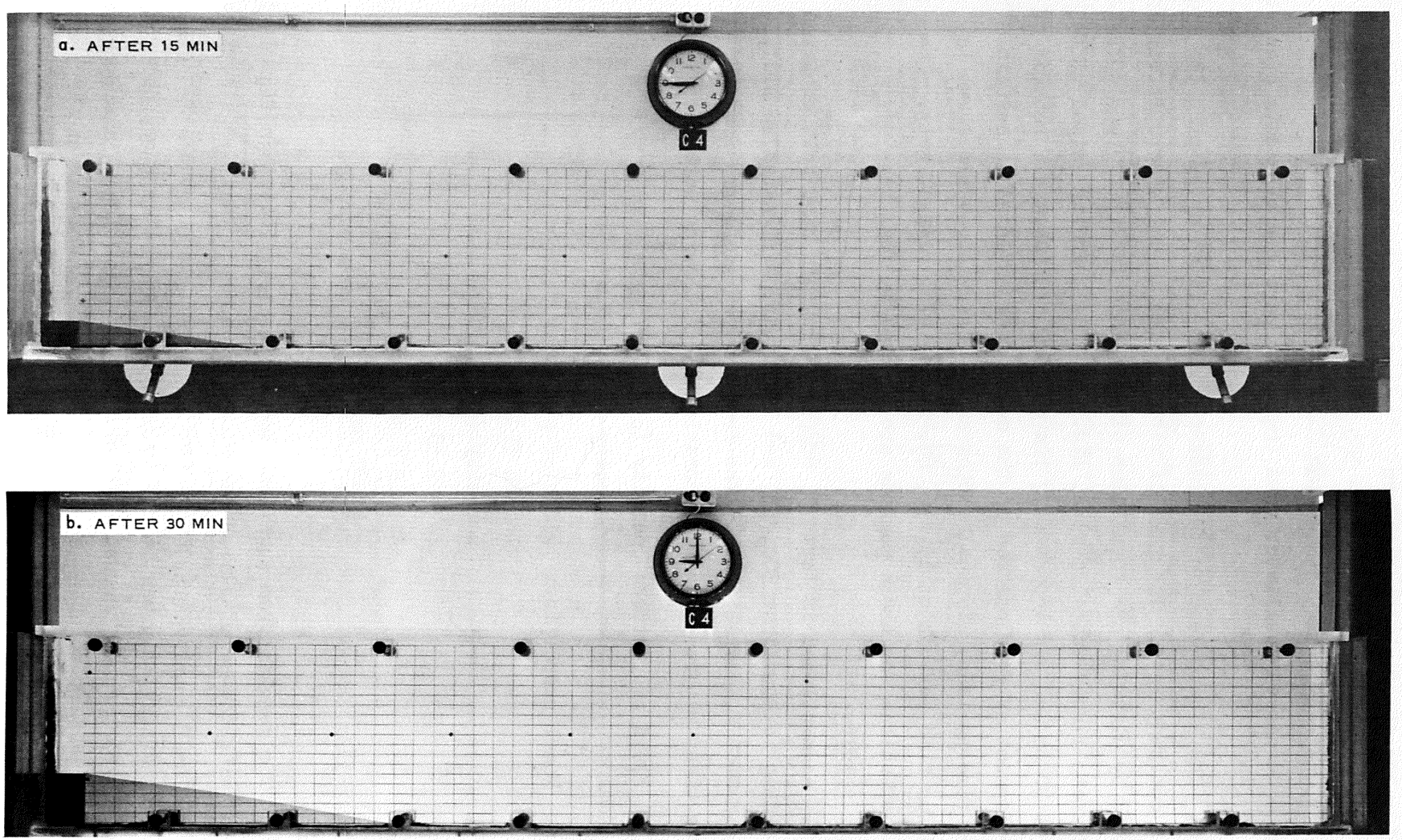

Fig. 12. Development of free surface in model (sheet 1 of 2)

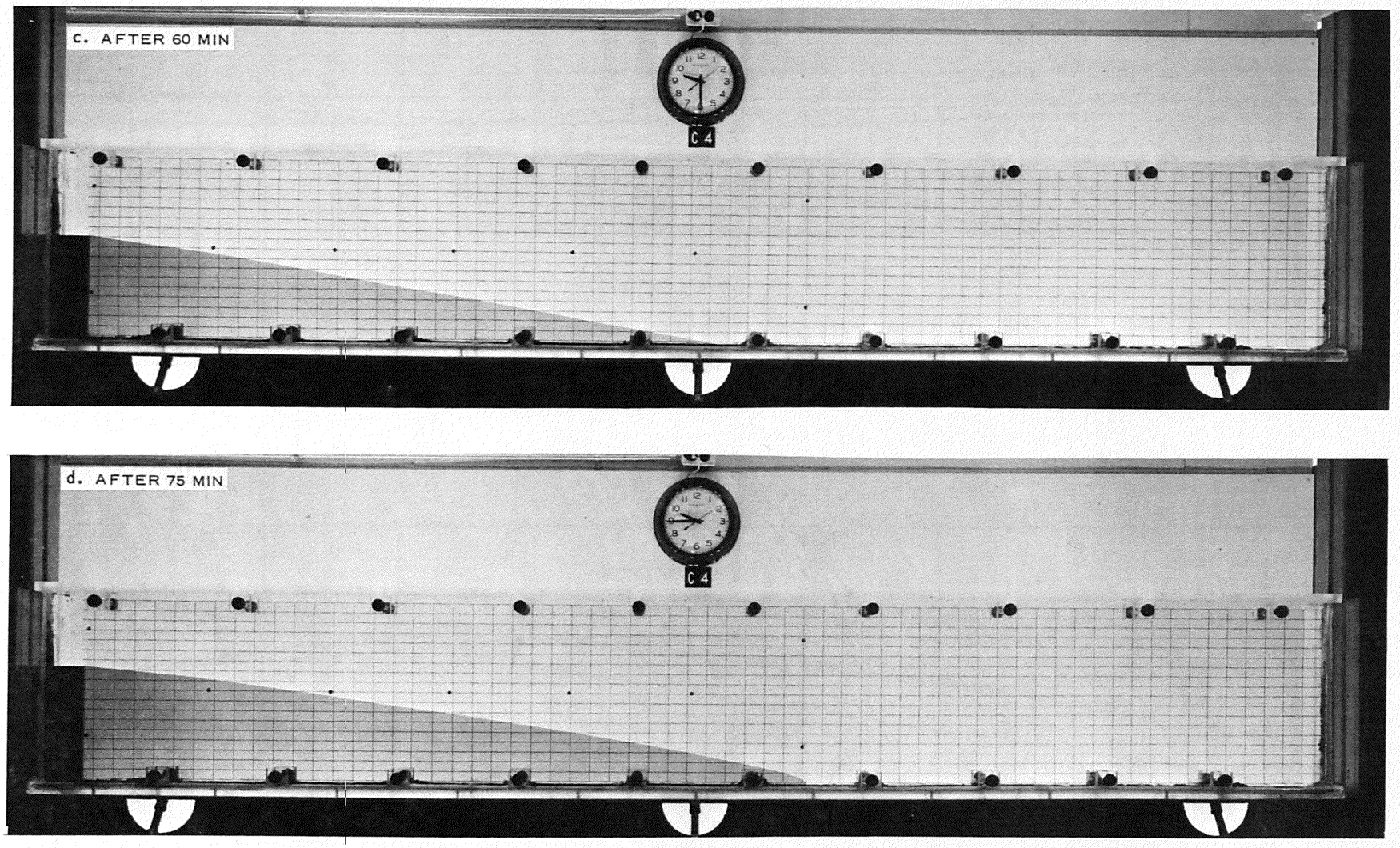

Fig. 12 (sheet 2 of 2)

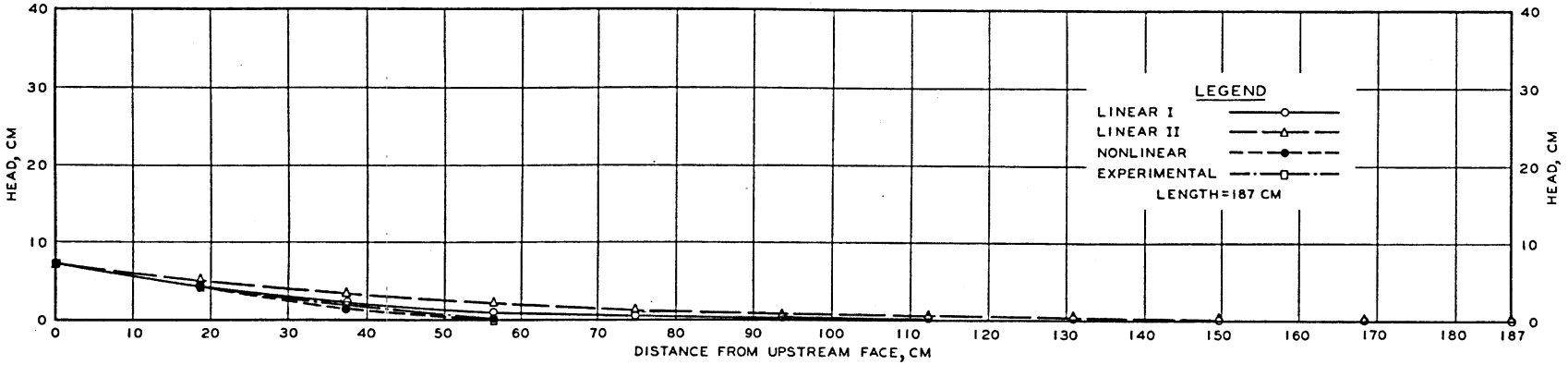

a. AFTER 15 MIN

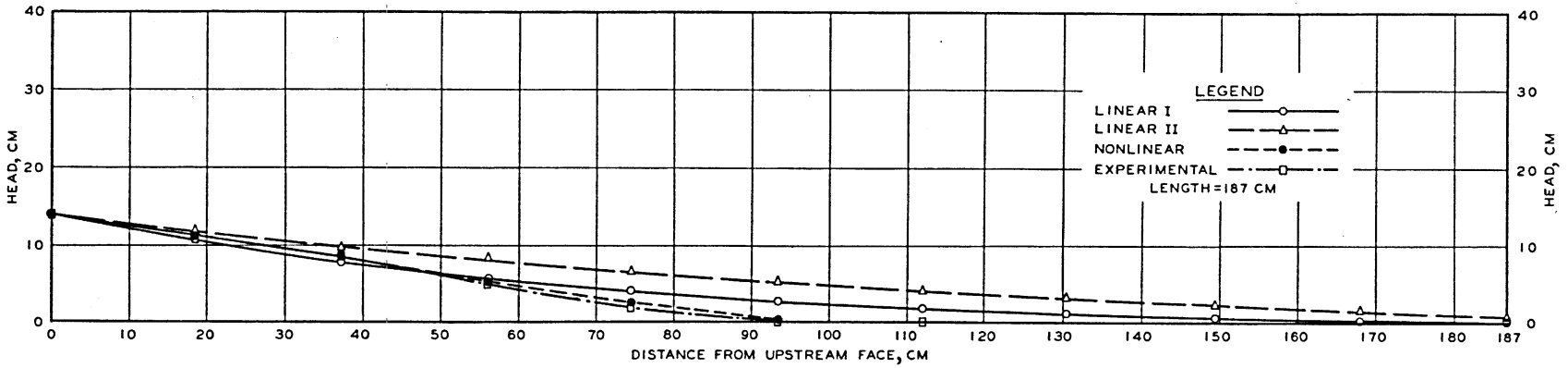

b. AFTER 30 MIN

Fig. 13. Head distributions, Test C_4 (sheet 1 of 2)

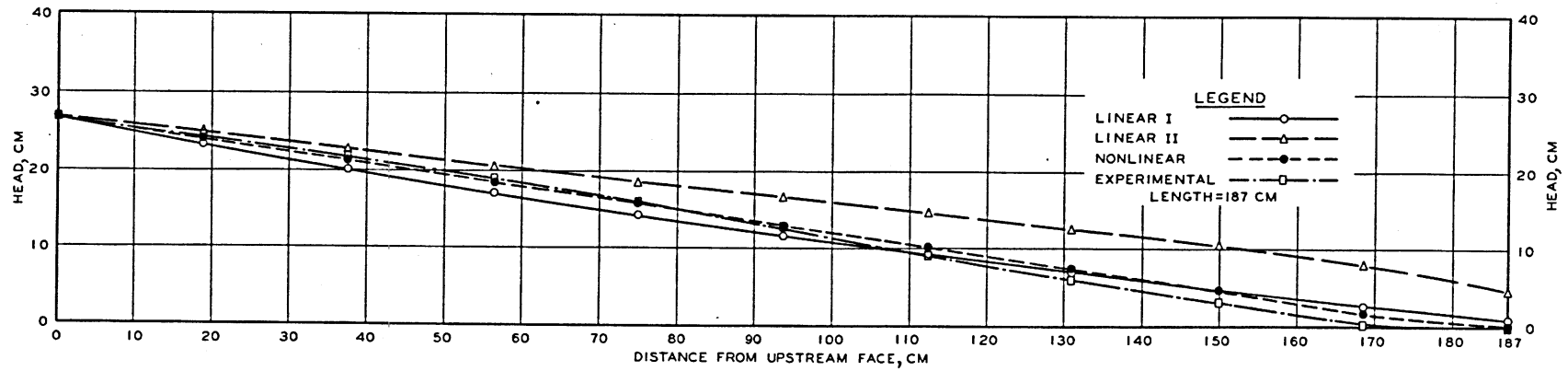

c. AFTER 60 MIN

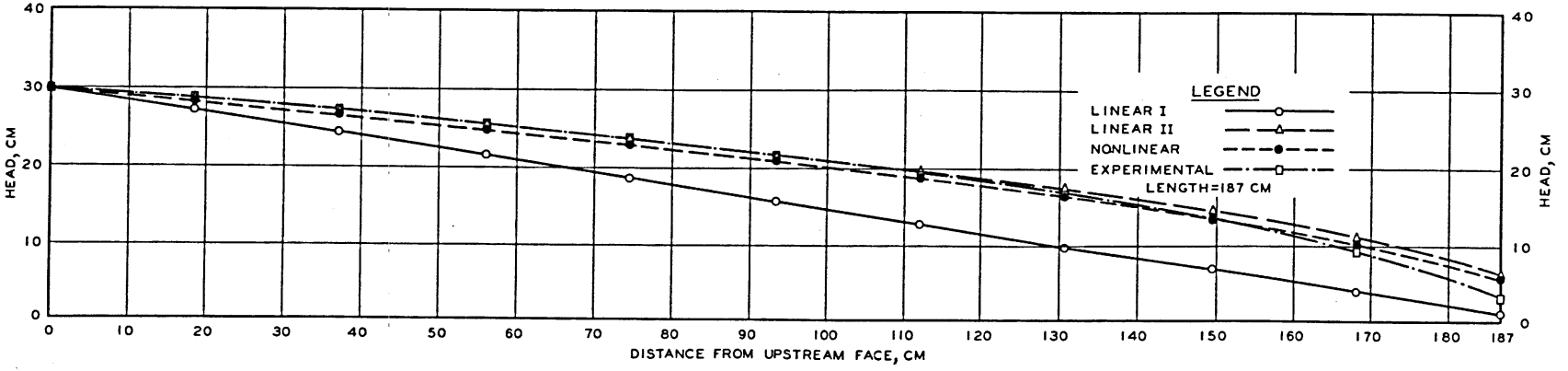

d. AFTER 75 MIN

Fig. 13 (sheet 2 of 2)

the assumption regarding head at the downstream boundary.

59. Satisfactory agreement is obtained between the results from LINI analysis and the experiment for times earlier than the time to reach the final head of 30 cm, fig. 13a, b, and c. In the steady state region, LINI results show large disagreement with experimental results, fig. 13d. This discrepancy may be due to the linear nature of the solution (equation 31) inherent in this formulation.

60. LINII analysis shows consistently higher results at earlier time periods (fig. 13a, b, and c), but indicates closer agreement in the steady state region (fig. 13d). This trend may be attributed to the parabolic nature[10] of the solution implied in this approximation.

61. Excellent agreement is obtained between the results from the NONLIN analysis and the experiments, fig. 13. The analytical and experimental curves lie very close to each other for all times and for the major portion of the length of the model. Some discrepancy is observed near the downstream region, and is believed to be due to the boundary approximation at the downstream face.

62. From overall estimation, it is concluded that the numerical approximations give reasonable and satisfactory results and that the approximation based on the nonlinear equation gives the most accurate results.

Sinusoidal river rise

63. The river at the upstream vertical face of the model is allowed to vary at a rate given by the function, fig. 14,

$$h(0,t) = \frac{h_o}{2} (1 - \cos \omega t) \qquad (40)$$

where h_o = maximum height of river. No experiments have been performed for this case, and only analytical results were obtained by using one of the computer programs (LINI). Maximum height h_o of 30 cm was adopted. This height was assumed to be reached in 1 hr,

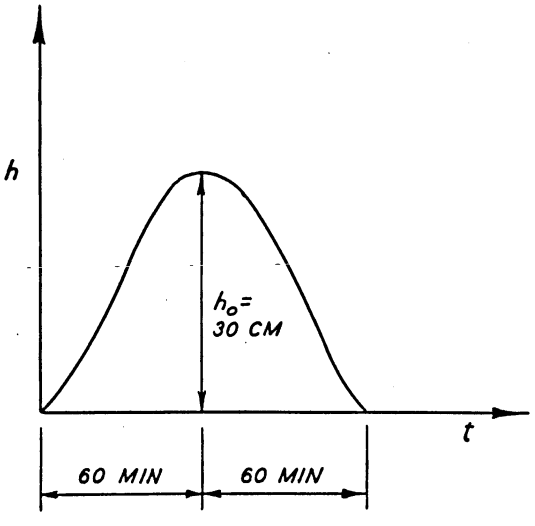

Fig. 14. Sinusoidal river rise

giving total period of flood as 2 hr. Beyond this time, the head at the upstream face is assumed to be zero. In the linearized equation, zero head gives the value of α equal to zero in equation 30c. Beyond the period of flood, therefore, the nonlinear equation 19 was cast into finite difference form stated below and was utilized to study the nature of the falling free surface after the time period of 2 hr.

$$\frac{h_i^{t+1} - h_i^t}{\Delta t} = \frac{b^2 \rho g}{3\mu n}\left[h_i^t\left(h_{i-1}^t - 2h_i^t + h_{i+1}^t\right) + \left(\frac{h_{i-1}^t - h_{i+1}^t}{2}\right)\right]$$

64. The results of this analysis are shown in fig. 15. The sequence of rise and fall of the free surface is indicated by numbers 1, 2, 3, and 6. It can be seen that in about 3 hr, most of the fluid flowed out of the model.

Two-Dimensional Flow

Experimental results

65. An experiment (series C_6) was conducted with the viscous flow model, adopting a plate length of 300 cm and an entrance slope of 45 deg. The width of gap between the plates was measured, and an average value of 0.17 cm was adopted. The head increased to a height of 30 cm at average rates as shown in fig. 16. The height of 30 cm was reached in 75 min and was maintained steady thereafter. Photographic records of the development of free surface were obtained for various time periods. Typical results for time periods of 15, 30, 60, and 120 min are shown in fig. 17 in comparison with the analytical results.

Analytical results

66. The permeability of the model was computed by using the equation

$$k_{model} = \frac{b^2 \rho g}{3\mu}$$

(The symbols are explained in paragraph 55.) The model dimensions were divided into a rectangular grid, 10 cm in size both in horizontal and vertical directions. For plate length of 300 cm, 30 intervals (Δx) were

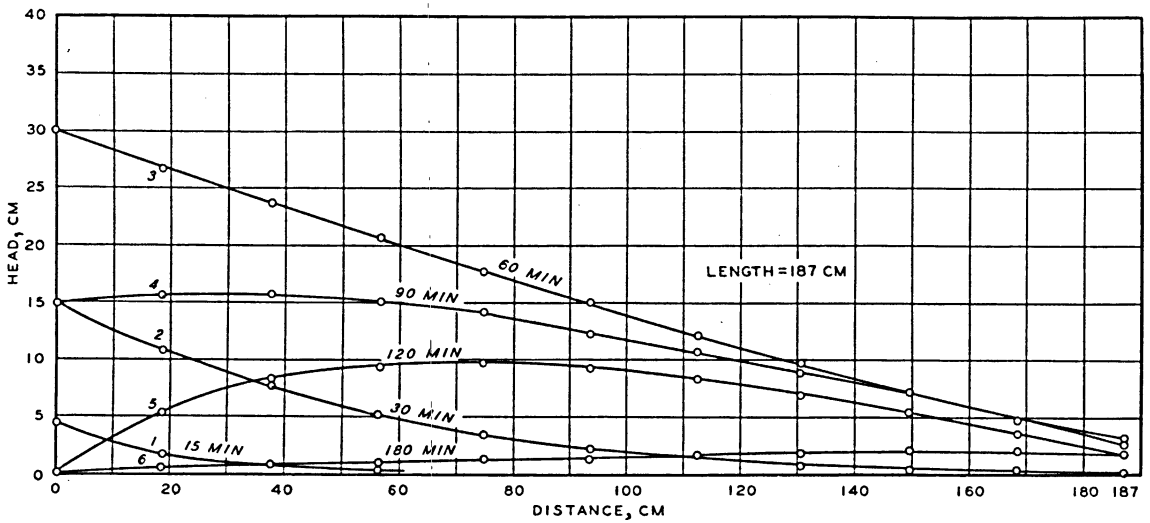

Fig. 15. Head distributions: sinusoidal flood

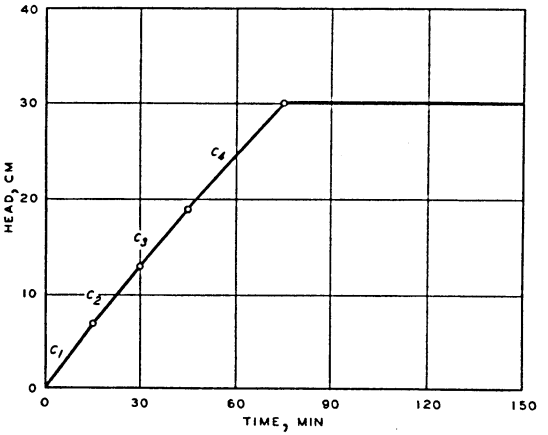

Fig. 16. Rise of river (Test C_6)

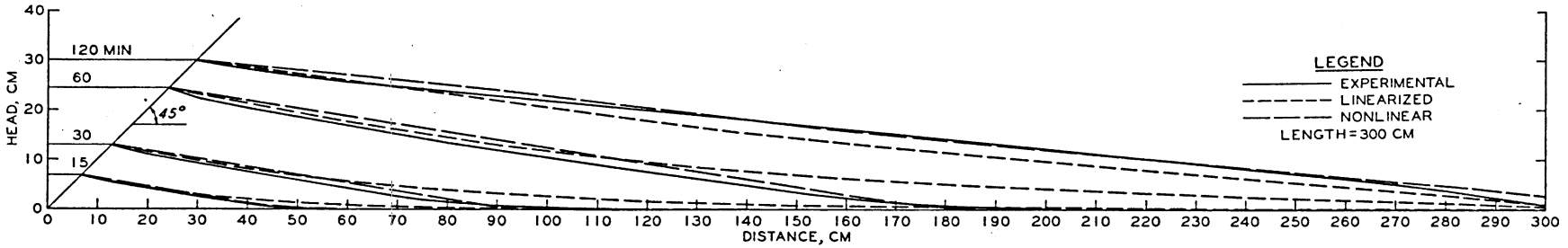

Fig. 17. Head distributions (α = 45 deg)

obtained in the horizontal direction, and 10 intervals (Δy) were chosen in the vertical direction. Numerical solutions in terms of heads at the nodes of the mesh were obtained by employing equation 38b for the boundary conditions given in paragraph 51. The free surface was then obtained by satisfying the condition that total head at the free surface is equal to the elevation. The free surfaces at time periods of 15, 30, 60, and 120 min are plotted in fig. 17.

Comparisons

67. Good agreement was obtained between the experimental and the analytical results for time periods of 15, 30, and 60 min (fig. 17). The difference between the curves in the regions nearer to the upstream face is small, but the difference increases at greater distances and near the base of the model. This difference may be attributed to the linearization process, the assumption of boundary conditions at the base and at the downstream end, and the friction at the base of the model. Although the analytical curves fail to intersect the impervious base of the model, equation 36, which does not permit $h = 0$ (for $x < \alpha$ and $t > 0$), the resulting solutions are on the side of safety with respect to stability analyses of the upstream slope; that is, the analytical solution will predict greater but not excessive pressures in the vicinity of the base than are existent.[11] The results indicate large discrepancy for longer time periods, fig. 17. This discrepancy is believed to be due to linearization of the basic governing equation.

68. Experiments with additional slope angles are in progress, and comparisons with analytical results will be obtained for these cases.

69. The overall estimation suggests that for two-dimensional flow the finite difference method may be conveniently used to obtain transient development of free surface. The free surface and the head distributions can then be used to draw flow nets and to compute the stability of banks.

70. As can be seen from fig. 17, the solutions obtained from the two-dimensional linearized equation show appreciable difference compared to the experimental results. Guided by a motivation from the better agreement between the solutions of the finite difference scheme in the nonlinear one-dimensional equation and the experiments, the finite difference scheme was

applied to the two-dimensional nonlinear equation (equation 25).

71. The two-dimensional nonlinear equation was obtained as

$$\frac{\partial h}{\partial t} = \frac{k_x}{n} \frac{\partial}{\partial x}\left(h \frac{\partial h}{\partial x}\right) + \frac{k_y}{n} h \frac{\partial^2 h}{\partial y^2} \qquad (25 \text{ bis})$$

or

$$\frac{\partial h}{\partial t} = \frac{k_x}{2n} \frac{\partial^2 h^2}{\partial x^2} + \frac{k_y}{n} h \frac{\partial^2 h}{\partial y^2} \qquad (41a)$$

Equation 41a was cast into finite difference form as

$$h_{i,j,t+1} = h_{i,j,t} + \frac{k_x \Delta t}{n(\Delta x_1 + \Delta x_2)}\left(\frac{h^2_{i-1,j,t+1} - h^2_{i,j,t+1}}{\Delta x_1} - \frac{h^2_{i,j,t} - h^2_{i+1,j,t}}{\Delta x_2}\right) + \frac{k_y \Delta t}{0.5n(\Delta y_1 + \Delta y_2)}\left(h_{i,j,t}\right) \times \left(\frac{h_{i,j+1,t+1} + h_{i,j,t+1}}{\Delta y_1} - \frac{h_{i,j,t} + h_{i,j-1,t}}{\Delta y_2}\right) \qquad (41b)$$

Equation 41b reduces to a quadratic form as

$$Ah^2_{i,j,t+1} + Bh_{i,j,t+1} + C = 0 \qquad (41c)$$

where A, B, and C are known quantities.

72. The results obtained employing equations 41b and 41c are plotted in fig. 17 for an upstream slope angle of 45 deg. It can be seen that the linearized solutions give closer agreement in the reaches in the vicinity of the upstream face of the model. However, the agreement shown by both linearized and nonlinear solutions with the experiments in these reaches is approximately similar. The main improvement of the nonlinear solution lies in its remarkably closer agreement with the experiments in the regions away from the upstream face and near to the impervious base. Also, at large times in the steady state zones represented by 120 min (fig. 17), the

linearized solution falls behind the experimental results, while the nonlinear solution again gives excellent agreement with the experiments. The above results suggest that the solutions obtained by incorporating the finite difference scheme in the special form of the nonlinear equation provide better numerical results.

PART VI: TRANSIENT SEEPAGE BY FINITE ELEMENT ANALYSIS

Formulation

73. The problem of transient flow in rigid porous media will be formulated by employing the finite element method. The linearized version of the governing differential equation for two-dimensional transient flow is given by

$$k_x \frac{\partial^2 h}{\partial x^2} + k_y \frac{\partial^2 h}{\partial y^2} = \frac{n}{\bar{h}} \frac{\partial h}{\partial t} \tag{42a}$$

where

h = potential

k_x, k_y = permeabilities in x and y directions, respectively

n = porosity

$\bar{h}$ = mean head

x, y = coordinate axes

t = time

Equation 42a can be expressed as

$$\nabla \cdot \underset{\approx}{k} \cdot \nabla \underset{\sim}{h} = \frac{n}{\bar{h}} \frac{\partial h}{\partial t} \tag{42b}$$

where

∇ = operator

$\underset{\approx}{k}$ = permeability matrix

The initial conditions may be in a form $\underset{\sim}{h}(x_i, 0) = \underset{\sim}{h}_o(x_i)$, where the index i denotes three coordinate directions 1, 2, and 3.

Development of Variational Principle

74. The variational principle for linear initial value problems was developed by Gurtin.[15] Wilson[16] used this principle for heat conduction problems and Javandel[17] used it for confined transient flow in porous media. Let u be a set of all functions $\underset{\sim}{h}(x_i, t)$ and their derivatives

be continuous over a given region of space R. For each $t\epsilon(0,\infty)$, define the functional

$$\Lambda_t(h) = \int_V \left(\frac{n}{\bar{h}} \underset{\sim}{h} * \underset{\sim}{h} + \nabla \underset{\sim}{h} * \underset{\approx}{k} * \nabla \underset{\sim}{h} - 2 \frac{n}{\bar{h}} \underset{\sim}{h}_o * \underset{\sim}{h} \right) dV - 2 \int_{B_1} \frac{\partial \underset{\sim}{h}}{\partial \eta} * \underset{\approx}{k} * \underset{\sim}{h} \, dB \quad (43)$$

where B_1 is the part of the boundary of R on which flow is specified. Potential is specified on the remainder of the boundary B.

75. The functional in equation 43 must assume a stationary value if $\underset{\sim}{h}$ is the solution to the following initial boundary value problem.

$$\nabla \cdot (\underset{\approx}{k} \nabla \underset{\sim}{h}) = \frac{n}{\bar{h}} \frac{\partial h}{\partial t} \quad (44)$$

With the boundary conditions

$$\underset{\sim}{h}(x_i) = \underset{\sim}{h}_o \quad \text{at} \quad t = 0$$

$$\underset{\sim}{h}(x_i) = \underset{\sim}{h}_1(x_i) \quad \text{on} \quad B_1$$

and

$$\bar{q}(x_i) = \frac{\partial \underset{\sim}{h}}{\partial \eta} * \underset{\approx}{k} \quad \text{on} \quad R - B_1$$

the above development implies that the initial value problem stated in equation 44 is equivalent to the problem of extremization of the functional in equation 43.

Finite Element Method

76. The finite element method involves systematic application of the Raleigh-Ritz procedure to a discretized continuum, and is fully discussed in literature;[18-21] hence, historical details of the method are not given here.

77. A porous medium is divided into a discrete number of pieces

called "finite elements." Unknown potentials are selected over an element, such that they vanish over the remaining elements. The potentials are assumed to be represented by an admissible polynomial in unknown potentials at the nodal points. As the shape and the dimensions of the elements may be arbitrarily chosen, any manner of boundary conditions can be treated. For a bank with infinite length, the flow may be treated as two-dimensional, and hence the method will be developed for two-dimensional flow conditions.

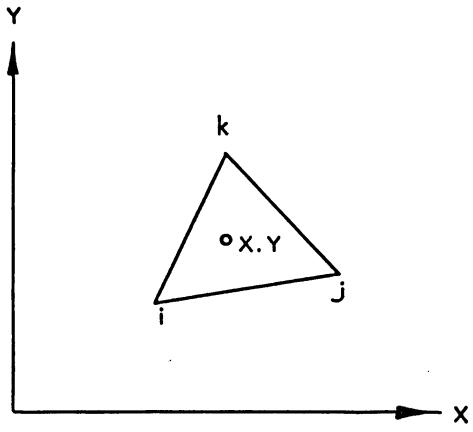

Fig. 18. Triangular finite element

78. A linear potential function is assumed and is expressed in terms of nodal point potentials, at the nodes i, j, and k , fig. 18. Let the function be given by

$$h(x_{i,t}) = \alpha + \beta x + \gamma y \tag{45a}$$

or

$$\begin{aligned} h_i &= \alpha + \beta x_i + \gamma y_i \\ h_j &= \alpha + \beta x_j + \gamma y_j \\ h_k &= \alpha + \beta x_k + \gamma y_k \end{aligned} \tag{45b}$$

or in matrix notation

$$\underset{\sim}{h} = \underline{\underline{A}}\ \underline{\alpha} \tag{45c}$$

where

$$\underset{\sim}{h} = \begin{bmatrix} h_i & h_j & h_k \end{bmatrix}^T$$

$$\underline{\underline{A}} = \begin{bmatrix} 1 & x_i & y_i \\ 1 & x_j & y_j \\ 1 & x_k & y_k \end{bmatrix}$$

and $\underline{\alpha} = \begin{bmatrix} \alpha & \beta & \gamma \end{bmatrix}^T$

Equation 45c can be written as:

$$\underset{\sim}{h} = \underset{\approx}{A}\,\underset{\sim}{\alpha} \tag{45d}$$

or

$$\underset{\sim}{\alpha} = \underset{\approx}{A}^{-1}\underset{\sim}{h} \tag{46a}$$

or

$$\underset{\sim}{\alpha} = \underset{\approx}{B}\,\underset{\sim}{h} \tag{46b}$$

where

$$\underset{\approx}{B} = \underset{\approx}{A}^{-1} = \frac{1}{\lambda}\begin{bmatrix} x_j y_k - x_k y_j & x_k y_i - x_i y_k & x_i y_j - x_j y_i \\ y_j - y_k & y_k - y_i & y_i - y_j \\ x_k - x_j & x_i - x_k & x_j - x_i \end{bmatrix}$$

where

$$\lambda = x_j(y_k - y_i) + x_i(y_j - y_k) + x_k(y_i - y_j)$$

79. Substituting equation 46b in equation 45d, the potential function in terms of nodal potentials is obtained as follows:

$$\underset{\sim}{h}_m(x_i,t) = \underset{\approx}{B}_m(x_i) \cdot \underset{\sim}{h}(t) \tag{47}$$

where

m denotes any element

$\underset{\sim}{h}(t)$ = column matrix of potentials at every nodal point

$\underset{\approx}{B}_m(x_i)$ = matrix dependent on coordinates of the nodal points

Differentiation of equation 47 with respect to the space coordinates yields

$$\left[\underset{\sim}{h}_m(x_i,t)\right]_{,i} = \underset{\approx}{D}_m(x_i)\underset{\sim}{h}(t) \tag{48}$$

where

$$\left[\underset{\sim}{h}_m(x_i,t)\right], \; i = \begin{bmatrix} \dfrac{\partial \underset{\sim}{h}_m}{\partial x}(x_i,t) \\ \dfrac{\partial \underset{\sim}{h}_m}{\partial y}(x_i,t) \end{bmatrix}$$

and

$$\underset{\approx}{D}_m(x_i) = \begin{bmatrix} \dfrac{\partial \underset{\approx}{B}_m}{\partial x}(x_i) \\ \dfrac{\partial \underset{\approx}{B}_m}{\partial y}(x_i) \end{bmatrix}$$

80. For the porous media divided into a number of finite elements, M , equation 43 can be expressed in summation form as

$$\Lambda_t(\underset{\sim}{h}) = \sum_{m=1}^{M} \int_{V_m} \left(\frac{n_m}{\bar{h}} \underset{\sim}{h}_m * \underset{\sim}{h}_m + \nabla \underset{\sim}{h}_m * \underset{\approx}{k} * \nabla \underset{\sim}{h}_m - 2 \frac{n_m}{\bar{h}} \underset{\sim}{h}_{om} * \underset{\sim}{h}_m \right) dV_m$$

$$- 2 \int_{B_{1m}} \frac{\partial \underset{\sim}{h}_m}{\partial \eta} * \underset{\approx}{k} * \underset{\sim}{h}_m \, dB_m \qquad (49)$$

Substituting equations 47 and 48 into equation 49 yields

$$\Lambda_t(\underset{\sim}{h}) = \sum_{m=1}^{M} \int_{V_m} \left\{ \frac{n_m}{\bar{h}} \left[\underset{\approx}{B}_m(x_i)\underset{\sim}{h}(t)\right]^T * \underset{\approx}{B}_m(x_i)\underset{\sim}{h}(t) \right.$$

$$+ \left[\underset{\approx}{D}(x_i)\underset{\sim}{h}(t)\right]^T * \underset{\approx}{k} * \underset{\approx}{D}_m(x_i)\underset{\sim}{h}(t)$$

$$\left. - 2 \frac{n_m}{\bar{h}} \left[\underset{\approx}{D}(x_i)\underset{\sim}{h}_{om}\right] * \left[\underset{\approx}{D}_m(x_i) \cdot \underset{\sim}{h}_t\right]^T \right\} dV_m$$

$$- 2 \int \left\{ \frac{\partial \underset{\sim}{h}_m}{\partial \eta} * \underset{\approx}{k} * \left[\underset{\approx}{B}_m(x_i) \cdot \underset{\sim}{h}_t\right]^T \right\} dV_m \qquad (50a)$$

or

$$\Lambda_t(\underset{\sim}{h}) = \sum_{m=1}^{M} \int_{V_m} \left[\frac{n_m}{\bar{h}} \underset{\sim}{h}^T_{(t)} \underset{\approx}{B}^T_m(x_i) * \underset{\approx}{B}_m(x_i) \underset{\sim}{h}(t) \right.$$

$$+ \underset{\sim}{h}^T_{(t)} \underset{\approx}{D}^T_m(x_i) * \underset{\approx}{k} * \underset{\approx}{D}_m(x_i) \underset{\sim}{h}(t)$$

$$\left. - 2 \frac{n_m}{\bar{h}} \underset{\sim}{h}^T(t) D_m(x_i)^T * \underset{\approx}{D}_m(x_i) \underset{\sim}{h}_{om} \right] dV_m$$

$$- 2 \int \left[\frac{\partial \underset{\sim}{h}_m}{\partial \eta} * \underset{\approx}{k} * \underset{\sim}{h}^T_t \underset{\approx}{B}^T_m(x_i) \right] dB_m \cdots \qquad (50b)$$

or

$$\Lambda_t(\underset{\sim}{h}) = \underset{\sim}{h}^T_{(t)} \underset{\approx}{P} * \underset{\sim}{h}_{(t)} + \underset{\sim}{h}^T_t * \bar{q} * \underset{\sim}{h}_{(t)}$$

$$- 2\underset{\sim}{h}^T_t \underset{\approx}{P} * \underset{\sim}{h}_o - 2\underset{\sim}{h}^T_t * \underset{\approx}{R} \cdots \qquad (50c)$$

where

$$\underset{\approx}{P} = \sum_{m=1}^{M} \int_{V_m} \frac{n_m}{\bar{h}} \underset{\approx}{B}^T_m(x_i) \cdot \underset{\approx}{B}_m(x_i) \, dV_m$$

$$\underset{\approx}{Q} = \sum_{m=1}^{M} \int_{V_m} \underset{\approx}{D}^T_m(x_i) \underset{\approx}{k} D_m(x_i)$$

$$\underset{\approx}{R} = \sum_{m=1}^{M} \int_{B_{lm}} \frac{\partial \underset{\sim}{h}_m}{\partial \eta} * \underset{\approx}{k} \underset{\approx}{D}^T_m(x_i) \, dB_m$$

where $\underset{\approx}{P}$, $\underset{\approx}{Q}$, and $\underset{\approx}{R}$ may be referred to as porosity, permeability, and fluid flow matrices, respectively.

81. For an extremum, the first variation of the functional in equation 50c must vanish; therefore,

$$\underset{\approx}{P}\,\underset{\sim}{h}_t + \underset{\approx}{Q} * \underset{\sim}{h}_t = \underset{\approx}{P}\,\underset{\sim}{h}_o + \underset{\approx}{R} \tag{51}$$

Equation 51 represents a set of linear equations in which the matrices $\underset{\approx}{P}$, $\underset{\approx}{Q}$, and $\underset{\approx}{R}$ are known and the potential $\underset{\sim}{h}_o$ is specified. Hence, solution of equation 51 will give values of $\underset{\sim}{h}$ at each nodal point in the discretized media.

82. Denoting $\underset{\sim}{h}_o$ by $\underset{\sim}{h}(t - \Delta t)$, equation 51 is expressed as

$$\underset{\approx}{P}\,\underset{\sim}{h}(t) + \underset{\approx}{Q} * \underset{\sim}{h}(t) = \underset{\approx}{P}\,\underset{\sim}{h}(t - \Delta t) + \underset{\approx}{R} \tag{52}$$

In this equation, the quantities involving convulsion products require integration in time coordinate. Since the variation of potential in time is unknown, linear variation will be assumed and small steps of time Δt adopted. This procedure is similar to Euler's one-step integration technique. Using this procedure, the following can be computed.

$$\underset{\approx}{Q} * \underset{\sim}{h}_t = \underset{\approx}{Q}\int_{t-\Delta t}^{t} \underset{\sim}{h}(\tau)\, d\tau$$

$$= \underset{\approx}{Q}\,\frac{\Delta t}{2}\left[\underset{\sim}{h}(t) + \underset{\sim}{h}\,(t - \Delta t)\right] \tag{53}$$

and

$$\underset{\approx}{R} = \frac{\Delta t}{2}\left[\underset{\approx}{q}(t) + \underset{\approx}{q}(t - \Delta t)\right] \tag{54}$$

Equation 52 now becomes

$$\underset{\approx}{P}\,\underset{\sim}{h}(t) + \underset{\approx}{Q}\,\frac{\Delta t}{2}\,\underset{\sim}{h}(t) + \underset{\approx}{Q}\,\frac{\Delta t}{2}\,\underset{\sim}{h}(t - \Delta t)$$

$$= \underset{\approx}{P}\,\underset{\sim}{h}(t - \Delta t) + \frac{\Delta t}{2}\,\underset{\approx}{q}(t) + \frac{\Delta t}{2}\,\underset{\approx}{q}(t - \Delta t) \ldots \tag{55}$$

By making the following substitutions,

$$\underset{\approx}{K} = \underset{\approx}{P} + \frac{\Delta t}{2}\,\underset{\approx}{Q}$$

$$\underset{\approx}{X} = \frac{1}{2}\left[\underset{\sim}{h}(t) + \underset{\sim}{h}(t - \Delta t)\right]$$

equation 55 can be rewritten as

$$\underset{\approx}{K}\,\underset{\sim}{X} = \underset{\approx}{P}\,\underset{\sim}{h}(t - \Delta t) + \frac{\Delta t}{4} \cdot \underset{\approx}{q}(t) + \frac{\Delta t}{4}\,\underset{\approx}{q}(t - \Delta t) \qquad (56)$$

Matrices $\underset{\approx}{K}$ and $\underset{\approx}{P}$ in equation 56 are functions only of the geometry of the elements and their physical properties and hence are known. If the rate of discharge $\underset{\approx}{q}$ is given, then equation 56 can be solved for $\underset{\sim}{X}$, which gives the values of potentials at the end of a time step. The procedure can be propagated in time by using the potentials just calculated as the initial potentials.

Application of Boundary Conditions

83. In a transient seepage problem, external head variation is generally known. The head either varies at a certain rate over the upstream boundary or remains constant. Assume that the head is prescribed on a face of the bank comprising M number of nodal points, out of total number of N nodal points. Equation 52 can then be written in a partitioned form as

$$\begin{bmatrix} \underset{\approx}{P}_{aa} & \underset{\approx}{P}_{ab} \\ M\times M & M\times(N-M) \\ \hline \underset{\approx}{P}_{ba} & \underset{\approx}{P}_{bb} \\ (N-M)\times M & (N-M)\times(N-M) \end{bmatrix} \begin{bmatrix} \underset{\sim}{h}_{a} \\ M\times 1 \\ \hline \underset{\sim}{h}_{b} \\ (N-M)\times 1 \end{bmatrix} + \begin{bmatrix} \underset{\approx}{Q}_{aa} & \underset{\approx}{Q}_{ab} \\ M\times M & M\times(N-M) \\ \hline \underset{\approx}{Q}_{ba} & \underset{\approx}{Q}_{bb} \\ (N-M)\times M & (N-M)\times(N-M) \end{bmatrix}$$

$$* \begin{bmatrix} \underset{\sim}{h}_{a} \\ M\times 1 \\ \hline \underset{\sim}{h}_{b} \\ (N-M)\times 1 \end{bmatrix} = \begin{bmatrix} \underset{\approx}{P}_{aa} & \underset{\approx}{P}_{ab} \\ M\times M & M\times(N-M) \\ \hline \underset{\approx}{P}_{ba} & \underset{\approx}{P}_{bb} \\ (N-M)\times M & (N-M)\times(N-M) \end{bmatrix} \begin{bmatrix} \underset{\sim}{h}_{a}(t-\Delta t) \\ M\times 1 \\ \hline \underset{\sim}{h}_{b}(t-\Delta t) \\ (N-M)\times 1 \end{bmatrix} + \begin{bmatrix} \underset{\sim}{R}_{a} \\ M\times 1 \\ \hline \underset{\sim}{R}_{b} \\ (N-M)\times 1 \end{bmatrix} \qquad (57)$$

84. The elements of $\underset{\sim}{h}_a$ are known, since the head at the upstream face is specified, and $\underset{\approx}{R}_a$ representing the flow at that face is unknown. Equation 47 can be expressed as:

$$\underset{\approx}{P}_{ba}\,\underset{\sim}{h}_a + \underset{\approx}{P}_{bb}\,\underset{\sim}{h}_b + \underset{\approx}{Q}_{ba} * \underset{\sim}{h}_a + \underset{\approx}{Q}_{bb} * \underset{\sim}{h}_b = \underset{\approx}{P}_{ba}\,\underset{\sim}{h}_a\,(t - \Delta t) + \underset{\approx}{P}_{bb}\,\underset{\sim}{h}_b\,(t - \Delta t) + \underset{\approx}{R}_b$$

or

$$\underset{\approx}{P}_{bb}\,\underset{\sim}{h}_b + \underset{\approx}{Q}_{bb} * \underset{\sim}{h}_b = \underset{\approx}{P}_{bb}\,h_b(t - \Delta t) + \underset{\approx}{S}_b \quad \ldots \tag{58}$$

where

$$\underset{\approx}{S}_b = \underset{\approx}{R}_b - \underset{\approx}{P}_{ba}\,\underset{\sim}{h}_a - \underset{\approx}{Q}_{ba} * h_a + \underset{\approx}{P}_{ba}\,\underset{\sim}{h}_a\,(t - \Delta t) \tag{59}$$

Equation 58 can now be solved for the unknown potentials $\underset{\sim}{h}_b$. If the quantity of flow at the upstream face is required, then $\underset{\approx}{R}_a$ can be computed as follows from equation 57.

$$\underset{\approx}{R}_a = \underset{\approx}{P}_{aa}\,\underset{\sim}{h}_a + \underset{\approx}{P}_{ab}\,h_b + \underset{\approx}{Q}_{aa} * \underset{\sim}{h}_a + \underset{\approx}{Q}_{ab} * h_b - \underset{\approx}{P}_{aa}\,h_a(t - \Delta t) - \underset{\approx}{P}_{ab}\,h_b(t - \Delta t) \tag{60}$$

PART VII: CONCLUSIONS AND RECOMMENDATIONS

Conclusions

85. The tests performed with the viscous flow model indicate that it provides an accurate, easy, and rapid means for solving transient seepage problems which cannot be solved by conventional means. The model can, however, only simulate relatively simple boundary conditions and material properties.

86. Numerical techniques are found to give satisfactory solutions and can account for arbitrary variation of material properties and complex boundary conditions encountered in riverbanks. The use of the finite difference scheme with the basic nonlinear equation of two-dimensional flow provides better solutions than the solutions from the linearized equation. Solutions obtained by employing the finite difference scheme agreed well with the results from model tests.

Recommendations

87. It is recommended that:

a. The finite difference scheme be used to obtain additional comparisons with experimental results for other upstream slope angles.

b. For more realistic simulation of field conditions, a mechanical device be installed in the model so as to allow both rise and fall in the river level with constant and sinusoidal rates.

88. Riverbanks, as they occur in nature, are generally heterogeneous in character and possess irregular boundaries. The finite difference method is convenient for simple stratification involving a small number of different materials and only for regular boundaries. It is therefore necessary to make recourse to the recently developed finite element method, since it can account for arbitrary variations in material properties and any manner of boundary shapes. It is proposed that computer programs be

developed for the finite element method, on the basis of the formulation obtained in this report.

LITERATURE CITED

1. Clough, G. W., "Ground Water Level in Silty and Sandy Mississippi River Upper Banks," Aug 1966, Mississippi River Commission, CE, Vicksburg, Miss.

2. Scheidegger, A. E., The Physics of Flow Through Porous Media, rev. ed., McMillan, New York, 1960.

3. Harr, M. E., Groundwater and Seepage, McGraw-Hill, New York, 1962.

4. Hele-Shaw, H. S., "Investigation of the Nature of Surface Resistance of Water and of Stream-Line Motion Under Certain Experimental Conditions," Transactions, Institution of Naval Architects, Vol 40, 1898, pp 21-46.

5. _____, "Stream-Line Motion of a Viscous Film," Report of the 68th Meeting of the British Association for the Advancement of Science, London, 1899, pp 136-142.

6. Todd, D. K., "Unsteady Flow in Porous Media by Means of a Hele-Shaw Viscous Fluid Model," Transactions, American Geophysical Union, Vol 35, No. 6, Dec 1954, pp 905-916.

7. Carslaw, H. S. and Jaeger, J. C., Conduction of Heat in Solids, 2d ed., Clarendon Press, Oxford, 1959.

8. Hantush, M. S., "Discussion of paper by P. P. Rowe, 'An Equation for Estimating Transmissibility and Coefficient of Storage from River-Level Fluctuations'," Journal of Geophysical Research, Vol 66, No. 4, Apr 1961, pp 1310-1311.

9. Cooper, H. H., Jr., and Rorabaugh, M. I., "Ground-Water Movements and Bank Storage Due to Flood Stages in Surface Stream," Water-Supply Paper 1536-J, 1963, U. S. Geological Survey, Washington, D. C.

10. Polubarinova-Kochina, P. Ya., Theory of Ground Water Movement, trans. from the Russian by J. M. Roger DeWiest, Princeton University Press, Princeton, N. J., 1962.

11. Brahma, S. P. and Harr, M. E., "Transient Development of the Free Surface in a Homogeneous Earth Dam," Geotechnique, Vol 12, No. 4, Dec 1962, pp 283-302.

12. Crandall, S. H., Engineering Analysis; A Survey of Numerical Procedures, McGraw-Hill, New York, 1956.

13. Terzidis, G., "Computational Schemes for the Boussinesq Equation," ASCE, Irrigation and Drainage Division, Journal, Vol 94, IR4, Dec 1968, pp 381-389.

14. Larkin, B. K., "Some Stable Explicit Difference Approximations to the Diffusion Equation," Mathematics of Computation, Vol 18, No. 86, Apr 1964.

15. Gurtin, M. E., "Variational Principles for Linear Initial Value Problems," Quarterly Applied Mathematics, Vol 22, 1964, p 2521.

16. Wilson, E. L. and Nickell, R. E., "Application of Finite Element Method to Heat Conduction Analysis," Nuclear Engineering and Design, North-Holland Publishing Company, Amsterdam, 1966, p 276.

17. Javandel, I. and Witherspoon, P. A., "Application of the Finite Element Method to Transient Flow in Porous Media," Transactions, American Institute of Mining, Metallurgical, and Petroleum Engineers, Vol 243, 1968.

18. Turner, M. J. et al., "Stiffness and Deflection Analysis of Complex Structures," Journal of Aeronautical Sciences, Vol 23, No. 9, Sept 1956, pp 805-823, 854.

19. Wilson, E. L., "Finite Element Analysis of Two-Dimensional Structures," Report No. 63-2, June 1963, Structural Engineering Laboratory, University of California, Berkeley, Calif.

20. Zienkiewicz, O. C. and Cheung, Y. K., The Finite Element Method in Structural and Continuum Mechanics; Numerical Solution of Problems in Structural and Continuum Mechanics, McGraw-Hill, New York, 1967.

21. Melosh, R. J., "Basis for Derivation of Matrices for Direct Stiffness Method," Journal, American Institute of Aeronautics and Astronautics, Vol 1, No. 7, July 1963, pp 1631-1637.

APPENDIX A: DERIVATION OF TWO-DIMENSIONAL FLOW EQUATION

1. Consider two-dimensional flow as in fig. A1. Unit width of the channel is considered for generality. The velocity components of flow in the x and y directions are denoted by u and v, respectively. The fluid surface rises by dh in time dt. The flows across faces 1-4 and 2-3 are given by

$$q_{x1} = u \times h \times 1 \tag{A1a}$$

$$q_{x2} = \left(u + \frac{\partial u}{\partial x}\, dx\right) \times \left(h + \frac{\partial h}{\partial x}\, dx\right) \times 1 \tag{A1b}$$

Therefore, net flow in x direction, ignoring higher order terms, is

$$q_x = -h \frac{\partial u}{\partial x}\, dx - u \frac{\partial h}{\partial x}\, dx \tag{A1c}$$

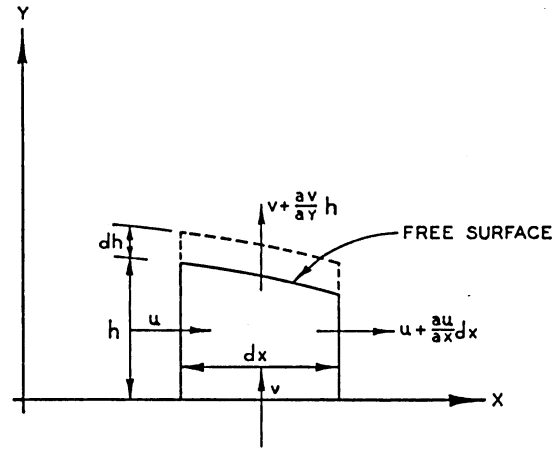

Fig. A1. Two-dimensional flow

Similarly, the flows across faces 1-2 and 3-4 are

$$q_{y1} = v \times dx \times 1 \tag{A2a}$$

$$q_{y2} = \left(v + \frac{\partial v}{\partial y}\, h\right) \times dx \times 1 \tag{A2b}$$

Net flow in y direction is

$$q_y = -h \frac{\partial v}{\partial y}\, dx \tag{A2c}$$

Net total flow change in time dt is

$$dq = -\left(h \frac{\partial u}{\partial x}\, dx + u \frac{\partial h}{\partial x}\, dx + h \frac{\partial v}{\partial y}\, dx\right) dt \tag{A3}$$

From Darcy's law, the relation between velocity and gradient can be expressed as

$$u = -k_x \frac{\partial h}{\partial x} \tag{A4a}$$

$$v = -k_y \frac{\partial h}{\partial y} \tag{A4b}$$

Therefore,

$$\frac{\partial u}{\partial x} = -k_x \frac{\partial^2 h}{\partial x^2} \tag{A4c}$$

$$\frac{\partial v}{\partial y} = -k_y \frac{\partial^2 h}{\partial y^2} \tag{A4d}$$

Substitution of equation A4 in equation A3 gives

$$q = \left\{ \left[h \frac{\partial^2 h}{\partial x^2} + \left(\frac{\partial h}{\partial x}\right)^2 \right] k_x + \left(h \frac{\partial^2 h}{\partial y^2} \right) k_y \right\} dx\, dt \tag{A5}$$

Now, assuming the flow to be incompressible, the change in the volume of the element in fig. A1 is

$$dv = n\, dx \frac{\partial h}{\partial t} dt \tag{A6}$$

and equating equations A5 and A6 yields

$$n \frac{\partial h}{\partial t} = k_x \left[h \frac{\partial^2 h}{\partial x^2} + \left(\frac{\partial h}{\partial x}\right)^2 \right] + k_y h \frac{\partial^2 h}{\partial y^2} \tag{A7a}$$

or

$$n \frac{\partial h}{\partial t} = k_x \frac{\partial}{\partial x} \left(h \frac{\partial h}{\partial x} \right) + k_y h \frac{\partial^2 h}{\partial y^2} \tag{A7b}$$

APPENDIX B: NONHOMOGENEOUS SOILS

1. Fig. B1a shows an inclined interface between two soils with permeabilities k_{x1} and k_{x2}. For convenience, an inclined interface is treated as a combination of horizontal and vertical interfaces.

Vertical Interface v-v

2. As shown in fig. B1b and c, v-v can occur either to the left or to the right of the node point (i,j). Linear head variation is assumed between nodes (i-1,j), (i,j), and (i+1,j). It is found necessary, as a numerical expedient, to establish a fictitious head h^* that represents head at node points (i-1,j), fig. B1b, or (i+1,j), fig. B1c, as if soil 2 and soil 1 were extending respectively into soil 1 and soil 2. An expression for h^* can then be substituted into the ADEP scheme as if the soils were homogeneous at the interface.

3. For v-v to the left of (i,j), fig. B1b, continuity of flow across v-v gives

$$k_{x1}\alpha_1 = k_{x2}\alpha_2 \tag{B1}$$

where α_1 and α_2 are shown in fig. B1b. Also, from linear head variation (time subscript is dropped for convenience),

$$\alpha_1(1 - \lambda)\Delta x1 + \alpha_2(\lambda + \beta_x)\Delta x1 = h_{i+1,j} - h_{i-1,j} \tag{B2}$$

Substitution of equation B1 into equation B2 gives

$$\alpha_1 = (h_{i+1,j} - h_{i-1,j}) \times \frac{1}{\Delta x1\left[(1 - \lambda) + k_{rx}(\lambda + \beta_x)\right]} \tag{B3}$$

where $k_{rx} = \dfrac{k_{x1}}{k_{x2}}$. Now,

$$h^*_{i-1,j} = h_{i-1,j} + (\alpha_1 - \alpha_2)(1 - \lambda)\Delta x1 \tag{B4}$$

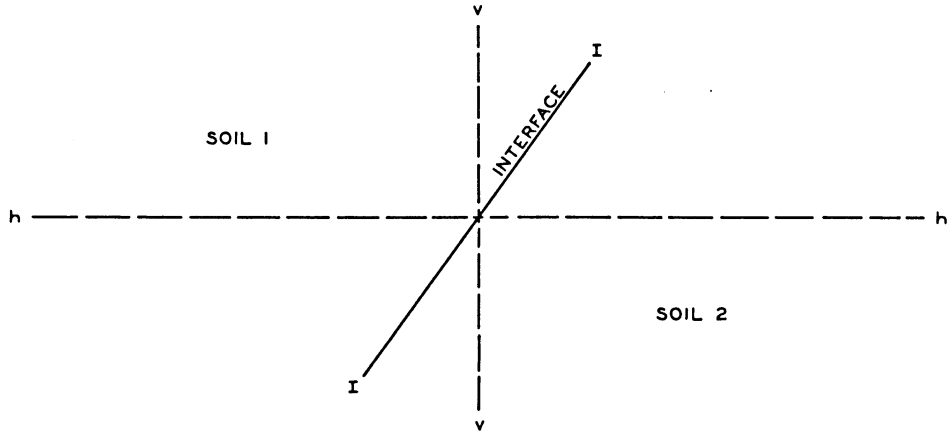

a. INCLINED INTERFACE

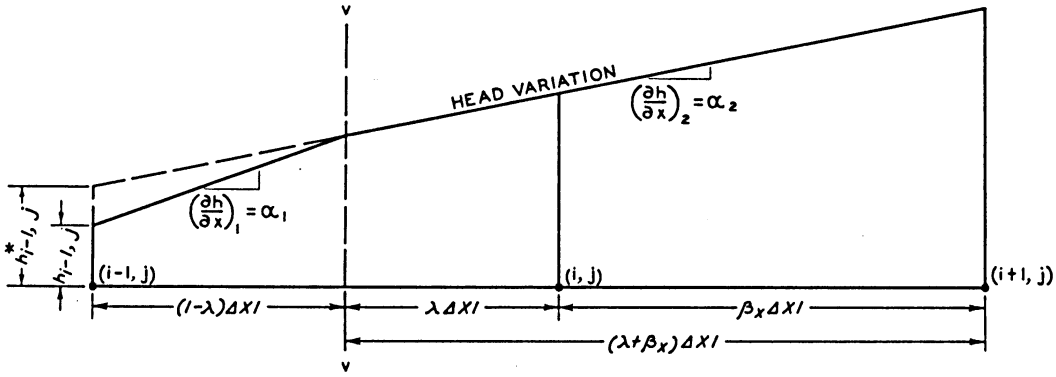

b. v-v TO LEFT OF (i, j)

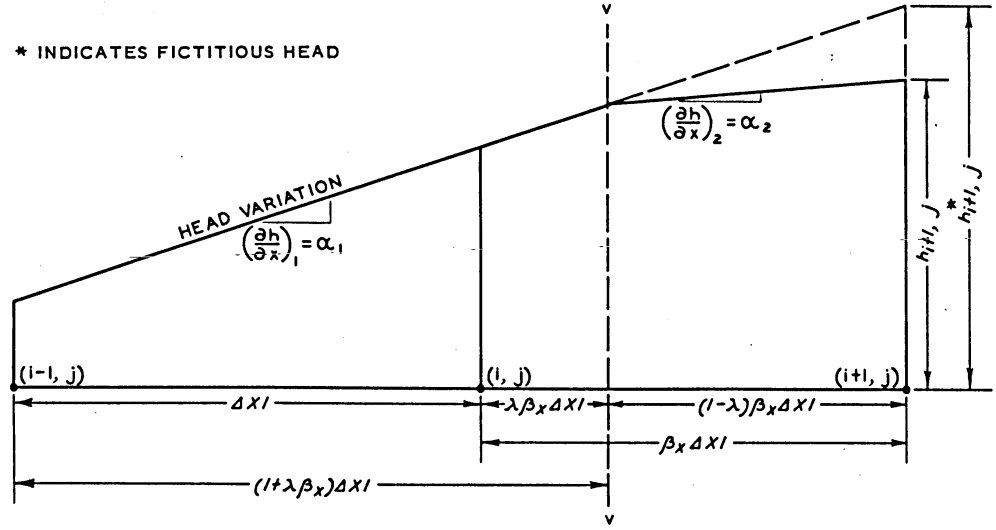

c. v-v TO RIGHT OF (i, j)

Fig. B1. Nonhomogeneous material

Substituting for α_1 and α_2, equation B4 becomes

$$h^*_{i-1,j} = h_{i-1,j} + (h_{i+1,j} - h_{i-1,j})\gamma_{x1} \tag{B5}$$

where $\gamma_{x1} = \dfrac{(1 - k_{rx})(1 - \lambda)}{(1 - \lambda) + k_{rx}(\lambda + \beta_x)}$. In a similar manner, for v-v to the right of (i,j), fig. B1c, the fictitious head is

$$h^*_{i+1,j} = h_{i+1,j} + (h_{i+1,j} - h_{i-1,j})\gamma_{x2} \tag{B6}$$

where $\gamma_{x2} = \dfrac{(1 - k_{rx})(1 - \lambda)}{(1 + \lambda\beta_x) + k_{rx}(1 - \lambda)\beta_x}$.

Horizontal Interface h-h

4. Following the similar procedure for h-h below and above the node point (i,j), the fictitious heads are, respectively,

$$h^*_{i,j-1} = h_{i,j-1} + (h_{i,j+1} - h_{i,j-1})\gamma_{y1} \tag{B7}$$

and

$$h^*_{i,j+1} = h_{i,j+1} + (h_{i,j+1} - h_{i,j-1})\gamma_{y2} \tag{B8}$$

where

$$\gamma_{y1} = \frac{(1 - k_{ry})(1 - \lambda)}{(1 - \lambda) + k_{ry}(\lambda + \beta_y)}$$

$$\gamma_{y2} = \frac{(1 - k_{ry})(1 - \lambda)}{(1 + \lambda\beta_y) + k_{ry}(1 - \lambda)\beta_y}$$

and

$$k_{ry} = \frac{k_{y1}}{k_{y2}}$$

5. The expressions for h^* can now be substituted in the ADEP scheme to account for any interface between two materials.

Unclassified

Security Classification

DOCUMENT CONTROL DATA - R & D

(Security classification of title, body of abstract and indexing annotation must be entered when the overall report is classified)

1. ORIGINATING ACTIVITY (Corporate author)	2a. REPORT SECURITY CLASSIFICATION
U. S. Army Engineer Waterways Experiment Station Vicksburg, Mississippi	Unclassified
	2b. GROUP

3. REPORT TITLE

SEEPAGE IN MISSISSIPPI RIVER BANKS; Report 1, ANALYSIS OF TRANSIENT SEEPAGE USING VISCOUS FLOW MODEL AND NUMERICAL METHODS

4. DESCRIPTIVE NOTES (Type of report and inclusive dates)

Report 1 of a series

5. AUTHOR(S) (First name, middle initial, last name)

Chandrakant S. Desai

6. REPORT DATE	7a. TOTAL NO. OF PAGES	7b. NO. OF REFS
February 1970	69	21

8a. CONTRACT OR GRANT NO.	9a. ORIGINATOR'S REPORT NUMBER(S)
b. PROJECT NO.	Miscellaneous Paper S-70-3, Report 1
c.	9b. OTHER REPORT NO(S) (Any other numbers that may be assigned this report)
d.	

10. DISTRIBUTION STATEMENT

This document has been approved for public release and sale; its distribution is unlimited.

11. SUPPLEMENTARY NOTES	12. SPONSORING MILITARY ACTIVITY
	U. S. Army Engineer Division, Lower Mississippi Valley, Vicksburg, Mississippi

13. ABSTRACT The design of stable riverbank slopes along the Mississippi River is dependent upon the seepage conditions within the banks generated by varying river level, including sudden drawdown. Available seepage analyses are not adequate for the determination of the continuously changing free-water surface under time-dependent variations in river levels. A parallel plate viscous flow model was constructed and tested and was found to constitute a reliable means of obtaining the transient free surface within a sloping bank. Two series of model tests were performed using a vertical upstream face and an upstream slope of 45 deg. The head at the upstream face of the model was allowed to rise at a constant rate. The experimental results are suitable only for simple boundary conditions and for homogeneous banks. It was, therefore, intended to develop some analytical techniques which can account for complex boundary conditions and nonhomogeneous material properties usually encountered in riverbanks. The finite difference and the finite element methods provide efficient numerical techniques for obtaining numerical solutions. The finite difference method was employed to obtain solutions for one- and two-dimensional flow conditions for a vertical riverbank and a sloping riverbank, respectively. To assess the applicability of the method for complex conditions, the numerical results were compared with those obtained from the experiments with the model for simple conditions. Good agreement was obtained between the two results. The basic formulation of the finite element method was developed and is included in this report. It is planned to develop some mechanical device to reproduce in the model various conditions of rise and fall of the river. It is recommended that programs for the finite difference and the finite element methods be further developed with an aim toward (a) providing complete solutions for complex boundary conditions and arbitrary variation of material properties encountered in riverbanks, and (b) simulating various types of river stage variations.

DD FORM 1 NOV 65 1473 REPLACES DD FORM 1473, 1 JAN 64, WHICH IS OBSOLETE FOR ARMY USE.

Unclassified

Security Classification

Unclassified

Security Classification

14. KEY WORDS	LINK A		LINK B		LINK C	
	ROLE	WT	ROLE	WT	ROLE	WT
Banks (waterways)						
Finite difference method						
Finite element method						
Mississippi River						
Models						
Numerical analysis						
Parallel plate viscous flow model						
Seepage						
Slopes						
Viscous flow						

Unclassified

Security Classification